MICROLITHOGRAPHY

Science and Technology

Second Edition

OPTICAL SCIENCE AND ENGINEERING

Founding Editor
Brian J. Thompson
University of Rochester
Rochester, New York

1. Electron and Ion Microscopy and Microanalysis: Principles and Applications, *Lawrence E. Murr*
2. Acousto-Optic Signal Processing: Theory and Implementation, *edited by Norman J. Berg and John N. Lee*
3. Electro-Optic and Acousto-Optic Scanning and Deflection, *Milton Gottlieb, Clive L. M. Ireland, and John Martin Ley*
4. Single-Mode Fiber Optics: Principles and Applications, *Luc B. Jeunhomme*
5. Pulse Code Formats for Fiber Optical Data Communication: Basic Principles and Applications, *David J. Morris*
6. Optical Materials: An Introduction to Selection and Application, *Solomon Musikant*
7. Infrared Methods for Gaseous Measurements: Theory and Practice, *edited by Joda Wormhoudt*
8. Laser Beam Scanning: Opto-Mechanical Devices, Systems, and Data Storage Optics, *edited by Gerald F. Marshall*
9. Opto-Mechanical Systems Design, *Paul R. Yoder, Jr.*
10. Optical Fiber Splices and Connectors: Theory and Methods, *Calvin M. Miller with Stephen C. Mettler and Ian A. White*
11. Laser Spectroscopy and Its Applications, *edited by Leon J. Radziemski, Richard W. Solarz, and Jeffrey A. Paisner*
12. Infrared Optoelectronics: Devices and Applications, *William Nunley and J. Scott Bechtel*
13. Integrated Optical Circuits and Components: Design and Applications, *edited by Lynn D. Hutcheson*
14. Handbook of Molecular Lasers, *edited by Peter K. Cheo*
15. Handbook of Optical Fibers and Cables, *Hiroshi Murata*
16. Acousto-Optics, *Adrian Korpel*
17. Procedures in Applied Optics, *John Strong*
18. Handbook of Solid-State Lasers, *edited by Peter K. Cheo*
19. Optical Computing: Digital and Symbolic, *edited by Raymond Arrathoon*
20. Laser Applications in Physical Chemistry, *edited by D. K. Evans*
21. Laser-Induced Plasmas and Applications, *edited by Leon J. Radziemski and David A. Cremers*
22. Infrared Technology Fundamentals, *Irving J. Spiro and Monroe Schlessinger*
23. Single-Mode Fiber Optics: Principles and Applications, Second Edition, Revised and Expanded, *Luc B. Jeunhomme*
24. Image Analysis Applications, *edited by Rangachar Kasturi and Mohan M. Trivedi*
25. Photoconductivity: Art, Science, and Technology, *N. V. Joshi*
26. Principles of Optical Circuit Engineering, *Mark A. Mentzer*
27. Lens Design, *Milton Laikin*

28. Optical Components, Systems, and Measurement Techniques, *Rajpal S. Sirohi and M. P. Kothiyal*
29. Electron and Ion Microscopy and Microanalysis: Principles and Applications, Second Edition, Revised and Expanded, *Lawrence E. Murr*
30. Handbook of Infrared Optical Materials, *edited by Paul Klocek*
31. Optical Scanning, *edited by Gerald F. Marshall*
32. Polymers for Lightwave and Integrated Optics: Technology and Applications, *edited by Lawrence A. Hornak*
33. Electro-Optical Displays, *edited by Mohammad A. Karim*
34. Mathematical Morphology in Image Processing, *edited by Edward R. Dougherty*
35. Opto-Mechanical Systems Design: Second Edition, Revised and Expanded, *Paul R. Yoder, Jr.*
36. Polarized Light: Fundamentals and Applications, *Edward Collett*
37. Rare Earth Doped Fiber Lasers and Amplifiers, *edited by Michel J. F. Digonnet*
38. Speckle Metrology, *edited by Rajpal S. Sirohi*
39. Organic Photoreceptors for Imaging Systems, *Paul M. Borsenberger and David S. Weiss*
40. Photonic Switching and Interconnects, *edited by Abdellatif Marrakchi*
41. Design and Fabrication of Acousto-Optic Devices, *edited by Akis P. Goutzoulis and Dennis R. Pape*
42. Digital Image Processing Methods, *edited by Edward R. Dougherty*
43. Visual Science and Engineering: Models and Applications, *edited by D. H. Kelly*
44. Handbook of Lens Design, *Daniel Malacara and Zacarias Malacara*
45. Photonic Devices and Systems, *edited by Robert G. Hunsberger*
46. Infrared Technology Fundamentals: Second Edition, Revised and Expanded, *edited by Monroe Schlessinger*
47. Spatial Light Modulator Technology: Materials, Devices, and Applications, *edited by Uzi Efron*
48. Lens Design: Second Edition, Revised and Expanded, *Milton Laikin*
49. Thin Films for Optical Systems, *edited by Francoise R. Flory*
50. Tunable Laser Applications, *edited by F. J. Duarte*
51. Acousto-Optic Signal Processing: Theory and Implementation, Second Edition, *edited by Norman J. Berg and John M. Pellegrino*
52. Handbook of Nonlinear Optics, *Richard L. Sutherland*
53. Handbook of Optical Fibers and Cables: Second Edition, *Hiroshi Murata*
54. Optical Storage and Retrieval: Memory, Neural Networks, and Fractals, *edited by Francis T. S. Yu and Suganda Jutamulia*
55. Devices for Optoelectronics, *Wallace B. Leigh*
56. Practical Design and Production of Optical Thin Films, *Ronald R. Willey*
57. Acousto-Optics: Second Edition, *Adrian Korpel*
58. Diffraction Gratings and Applications, *Erwin G. Loewen and Evgeny Popov*
59. Organic Photoreceptors for Xerography, *Paul M. Borsenberger and David S. Weiss*
60. Characterization Techniques and Tabulations for Organic Nonlinear Optical Materials, *edited by Mark G. Kuzyk and Carl W. Dirk*
61. Interferogram Analysis for Optical Testing, *Daniel Malacara, Manuel Servin, and Zacarias Malacara*
62. Computational Modeling of Vision: The Role of Combination, *William R. Uttal, Ramakrishna Kakarala, Spiram Dayanand, Thomas Shepherd, Jagadeesh Kalki, Charles F. Lunskis, Jr., and Ning Liu*
63. Microoptics Technology: Fabrication and Applications of Lens Arrays and Devices, *Nicholas Borrelli*
64. Visual Information Representation, Communication, and Image Processing, *edited by Chang Wen Chen and Ya-Qin Zhang*
65. Optical Methods of Measurement, *Rajpal S. Sirohi and F. S. Chau*

66. Integrated Optical Circuits and Components: Design and Applications, *edited by Edmond J. Murphy*
67. Adaptive Optics Engineering Handbook, *edited by Robert K. Tyson*
68. Entropy and Information Optics, *Francis T. S. Yu*
69. Computational Methods for Electromagnetic and Optical Systems, *John M. Jarem and Partha P. Banerjee*
70. Laser Beam Shaping, *Fred M. Dickey and Scott C. Holswade*
71. Rare-Earth-Doped Fiber Lasers and Amplifiers: Second Edition, Revised and Expanded, *edited by Michel J. F. Digonnet*
72. Lens Design: Third Edition, Revised and Expanded, *Milton Laikin*
73. Handbook of Optical Engineering, *edited by Daniel Malacara and Brian J. Thompson*
74. Handbook of Imaging Materials: Second Edition, Revised and Expanded, *edited by Arthur S. Diamond and David S. Weiss*
75. Handbook of Image Quality: Characterization and Prediction, *Brian W. Keelan*
76. Fiber Optic Sensors, *edited by Francis T. S. Yu and Shizhuo Yin*
77. Optical Switching/Networking and Computing for Multimedia Systems, *edited by Mohsen Guizani and Abdella Battou*
78. Image Recognition and Classification: Algorithms, Systems, and Applications, *edited by Bahram Javidi*
79. Practical Design and Production of Optical Thin Films: Second Edition, Revised and Expanded, *Ronald R. Willey*
80. Ultrafast Lasers: Technology and Applications, *edited by Martin E. Fermann, Almantas Galvanauskas, and Gregg Sucha*
81. Light Propagation in Periodic Media: Differential Theory and Design, *Michel Nevière and Evgeny Popov*
82. Handbook of Nonlinear Optics, Second Edition, Revised and Expanded, *Richard L. Sutherland*
83. Polarized Light: Second Edition, Revised and Expanded, *Dennis Goldstein*
84. Optical Remote Sensing: Science and Technology, *Walter Egan*
85. Handbook of Optical Design: Second Edition, *Daniel Malacara and Zacarias Malacara*
86. Nonlinear Optics: Theory, Numerical Modeling, and Applications, *Partha P. Banerjee*
87. Semiconductor and Metal Nanocrystals: Synthesis and Electronic and Optical Properties, edited by *Victor I. Klimov*
88. High-Performance Backbone Network Technology, *edited by Naoaki Yamanaka*
89. Semiconductor Laser Fundamentals, *Toshiaki Suhara*
90. Handbook of Optical and Laser Scanning, *edited by Gerald F. Marshall*
91. Organic Light-Emitting Diodes: Principles, Characteristics, and Processes, *Jan Kalinowski*
92. Micro-Optomechatronics, *Hiroshi Hosaka, Yoshitada Katagiri, Terunao Hirota, and Kiyoshi Itao*
93. Microoptics Technology: Second Edition, *Nicholas F. Borrelli*
94. Organic Electroluminescence, *edited by Zakya Kafafi*
95. Engineering Thin Films and Nanostructures with Ion Beams, *Emile Knystautas*
96. Interferogram Analysis for Optical Testing, Second Edition, *Daniel Malacara, Manuel Servin, and Zacarias Malacara*
97. Laser Remote Sensing, *edited by Takashi Fujii and Tetsuo Fukuchi*
98. Passive Micro-Optical Alignment Methods, *edited by Robert A. Boudreau and Sharon M. Boudreau*
99. Organic Photovoltaics: Mechanism, Materials, and Devices, *edited by Sam-Shajing Sun and Niyazi Serdar Sariciftci*
100. Handbook of Optical Interconnects, *edited by Shigeru Kawai*
101. GMPLS Technologies: Broadband Backbone Networks and Systems, *Naoaki Yamanaka, Kohei Shiomoto, and Eiji Oki*

102. Laser Beam Shaping Applications, *edited by Fred M. Dickey, Scott C. Holswade and David L. Shealy*
103. Electromagnetic Theory and Applications for Photonic Crystals, *Kiyotoshi Yasumoto*
104. Physics of Optoelectronics, *Michael A. Parker*
105. Opto-Mechanical Systems Design: Third Edition, *Paul R. Yoder, Jr.*
106. Color Desktop Printer Technology, *edited by Mitchell Rosen and Noboru Ohta*
107. Laser Safety Management, *Ken Barat*
108. Optics in Magnetic Multilayers and Nanostructures, *Štefan Višňovský*
109. Optical Inspection of Microsystems, *edited by Wolfgang Osten*
110. Applied Microphotonics, *edited by Wes R. Jamroz, Roman Kruzelecky, and Emile I. Haddad*
111. Organic Light-Emitting Materials and Devices, *edited by Zhigang Li and Hong Meng*
112. Silicon Nanoelectronics, *edited by Shunri Oda and David Ferry*
113. Image Sensors and Signal Processor for Digital Still Cameras, *Junichi Nakamura*
114. Encyclopedic Handbook of Integrated Circuits, *edited by Kenichi Iga and Yasuo Kokubun*
115. Quantum Communications and Cryptography, *edited by Alexander V. Sergienko*
116. Optical Code Division Multiple Access: Fundamentals and Applications, *edited by Paul R. Prucnal*
117. Polymer Fiber Optics: Materials, Physics, and Applications, *Mark G. Kuzyk*
118. Smart Biosensor Technology, *edited by George K. Knopf and Amarjeet S. Bassi*
119. Solid-State Lasers and Applications, *edited by Alphan Sennaroglu*
120. Optical Waveguides: From Theory to Applied Technologies, *edited by Maria L. Calvo and Vasudevan Lakshiminarayanan*
121. Gas Lasers, *edited by Masamori Endo and Robert F. Walker*
122. Lens Design, Fourth Edition, *Milton Laikin*
123. Photonics: Principles and Practices, *Abdul Al-Azzawi*
124. Microwave Photonics, *edited by Chi H. Lee*
125. Physical Properties and Data of Optical Materials, *Moriaki Wakaki, Keiei Kudo, and Takehisa Shibuya*
126. Microlithography: Science and Technology, Second Edition, *edited by Kazuaki Suzuki and Bruce W. Smith*

MICROLITHOGRAPHY

Science and Technology

Second Edition

edited by

Kazuaki Suzuki
Bruce W. Smith

CRC Press
Taylor & Francis Group
Boca Raton London New York

CRC Press is an imprint of the
Taylor & Francis Group, an informa business

CRC Press
Taylor & Francis Group
6000 Broken Sound Parkway NW, Suite 300
Boca Raton, FL 33487-2742

CRC Press is an imprint of Taylor & Francis Group, an Informa business

No claim to original U.S. Government works
Printed in the United States of America on acid-free paper
10 9 8 7 6 5 4 3 2 1

International Standard Book Number-10: 0-8247-9024-3 (Hardcover)
International Standard Book Number-13: 978-0-8247-9024-0 (Hardcover)

Library of Congress Cataloging-in-Publication Data

Microlithography : science and technology / editors, Kazuaki Suzuki and Bruce W. Smith. -- 2nd ed.
p. cm. -- (Optical science and engineering series)
"A CRC title."
Includes bibliographical references and index.
ISBN-13: 978-0-8247-9024-0 (alk. paper)
ISBN-10: 0-8247-9024-3 (alk. paper)
1. Microlithography--Industrial applications. 2. Integrated circuits--Masks. 3. Metal oxide semiconductors, Complementary--Design and construction. 4. Manufacturing processes. I. Suzuki, Kazuaki. II. Smith, Bruce W., 1959-

TK7836.M525 2007
621.3815'31--dc22 2006031516

Visit the Taylor & Francis Web site at
http://www.taylorandfrancis.com

and the CRC Press Web site at
http://www.crcpress.com

Preface

Over the last three decades, accomplishments in microlithographic technology have resulted in tremendous advances in the development of semiconductor integrated circuits (ICs) and microelectromechanical systems (MEMS). As a direct result, devices have become both faster and smaller, can handle an ever increasing amount of information, and are used in applications from the purely scientific to those of everyday life. With the shrinking of device patterns approaching the nanometer scale, the wavelength of the exposing radiation has been reduced from the blue-UV wavelength of the mercury *g*-line (436 nm) into the mercury *i*-line(365 nm), deep UV (DUV), vacuum UV (VUV), and the extreme UV (EUV). The krypton fluoride (KrF) excimer laser at 248 nm was adopted as an exposure source in DUV regions and has been used in volume manufacturing since 1988.

Since the first edition of this book, advances in 193-nm argon flouride (ArF) excimer laser lithography have allowed for the pursuit of sub-90-nm device fabrication and, when combined with high NA technology, polarized illumination, and immersion imaging, may be capable of imaging for device generations at 45 nm and beyond. The next generation of lithographic systems for 32-nm device technology will likely come from candidates including F_2 excimer laser (157 nm) lithography, EUV (13.5 nm) lithography, electron projection lithography (EPL), nanoimprint lithography (NIL), or maskless lithography (ML2). Among these candidates, ML2 such as electron-beam direct-write system has been used for small-volume device production with quick turn around time (QTAT) because a mask is not necessary. Factors that will determine the ultimate course for a high-volume device production will include cost, throughput, resolution, and extendibility to finer resolution.

The second edition of this volume is written not only as an introduction to the science and technology of microlithography, but also as a reference for those who with more experience so that they may obtain a wider knowledge and a deeper understanding of the field. The purpose of this update remains consistent with the first edition published in 1998 and edited by Dr. James R. Sheats and Dr. Bruce W. Smith. New advances in lithography have required that we update the coverage of microlithography systems and approaches, as well as resist materials, processes, and metrology techniques.

The contributors were organized and revision work started in 2003. Additional content and description have been added regarding immersion lithography, 157-nm lithography and EPL in Chapter 1 *System Overview of Optical Steppers and Scanners*, Chapter 3 *Optics for Photolithograph*, Chapter 5 *Excimer Laser for Advanced Microlithography*, and Chapter 6 *Electron Beam Lithography Systems*. Because the topics of EUV and imprint lithography were not addressed in the first edition, Chapter 8 and Chapter 9 have been added to discuss these as well. A detailed explanation of scatterometry has been incorporated into Chapter 14 *Critical Dimensional Metrology*. Chapter 15 *Electron Beam Nanolithography* has also has been widely revised. In order to maintain the continuity of this textbook, that proved so valuable in the first edition, these topics and others that may be less obvious, but no less significant, have been tied into the other corresponding chapters as necessary. As a result, we are certain that this second edition of *Microlithography: Science and Technology* will remain a valuable textbook for students, engineers, and researchers and will be a useful resource well into the future.

Kazuaki Suzuki
Bruce W. Smith

Editors

Kazuaki Suzuki is a project manager of Next Generation Lithography Tool Development at the Nikon Corporation. He has joined several projects of new concept exposure tools such as the first generation KrF excimer laser stepper, the first generation KrF excimer laser scanner, the electron-beam projection lithography system, and the full field EUV scanner. He has authored and coauthored many papers in the field of exposure tools and related technologies. He also holds numerous patents in the areas of projection lens control systems, dosage control systems, focusing control systems, and evaluation methods for image quality. For the last several years, he has been a member of program committees such as SPIE Microlithography and other international conferences. He is an associate editor of The Journal of Micro/Nanolithography, MEMS, and MOEMS (JM3). Kazuaki Suzuki received his BS degree in plasma physics (1981), and his MS degree in x-ray astronomy (1983) from Tokyo University, Japan. He retired from a doctorate course in x-ray astronomy and joined the Nikon Corporation in 1984.

Bruce W. Smith is a professor of microelectronic engineering and the director of the Center for Nanolithography Research at the Rochester Institute of Technology. He is involved in research in the fields of DUV and VUV lithography, photoresist materials, resolution enhancement technology, aberration theory, optical thin film materials, illumination design, immersion lithography, and evanescent wave imaging. He has authored numerous scientific publications and holds several patents. Dr. Smith is a widely known educator in the field of optical microlithography. He received his MS degree and doctorate in imaging science from the Rochester Institute of Technology. He is a member of the International Society for Photo-optical Instrumentation Engineering (SPIE), the Optical Society of America (OSA), and the Institute of Electrical and Electronics Engineers (IEEE).

Contributors

Mike Adel KLA-Tencor, Israel

Robert D. Allen IBM Almaden Research Center, San Jose, California

Zvonimir Z. Bandić Hitachi San Jose Research Center, San Jose, California

Palash Das Cymer, Inc., San Diego, California

Elizabeth A. Dobisz Hitachi San Jose Research Center, San Jose, California

Gregg M. Gallatin IBM Thomas J. Watson Research Center, Yorktown Heights, New York (Current Affiliation: Applied Math Solutions, LLC, Newton, Connecticut)

Charles Gwyn Intel Corporation (Retired)

Maureen Hanratty Texas Instruments, Dallas, Texas

Michael S. Hibbs IBM Microelectronic Division, Essex Junction, Vermont

Roderick R. Kunz Massachusetts Institute of Technology, Lexington, Massachusetts

Gian Lorusso IMEC, Leuven, Belgium

Chris A. Mack KLA-Tencor FINLE Divison, Austin, Texas (Retired, Currently Gentleman Scientist)

Herschel M. Marchman KLA-Tencor, San Jose, California (Current Affiliation: Howard Hughes Medical Institute, Ashburn, Virginia)

Martin C. Peckerar University of Maryland, College Park, Maryland

Douglas J. Resnick Motorola, Tempe, Arizona (Current Affiliation: Molecular Imprints, Austin, Texas)

Bruce W. Smith Rochester Institute of Technology, Rochester, New York

Kazuaki Suzuki Nikon Corporation, Saitama, Japan

Takumi Ueno Hitachi Chemical Electronic Materials R&D Center, Ibaraki, Japan

Stefan Wurm International SEMATECH (Qimonda assignee), Austin, Texas

Sanjay Yedur Timbre Technologies Inc., a division of Tokyo Electron Limited, Santa Clara, California

Contents

Part III Metrology and Nanolithography

12

Multilayer Resist Technology

Bruce W. Smith and Maureen Hanratty

CONTENTS

12.1 Introduction

As higher-resolution approaches to microlithography are pursued, conventional single-layer resist materials may fail to meet all process requirements. Multilayer resist techniques have been investigated for several years, but advances in single-layer technology have generally postponed their insertion into high-volume production operations. As long as single-layer resist materials can meet requirements for high-aspect-ratio resolution, photosensitivity, plasma-etch resistance, planarization, depth of focus, reflection control, and critical dimension (CD) control, they will be preferred over most multiple-layer or pseudo-multiple-layer techniques. This becomes increasingly difficult and, at some point, the lithographer needs to consider the advantages of dividing the functions of a single-layer resist into separate layers. Fewer layers are better and the ultimate acceptance of any multiplayer technique will be determined by the simplicity of the overall process.

To understand the potential advantages of multiple-layer lithographic materials and processes, the general requirements of a photoresist should first be addressed. Although most resist requirements have existed for many generations of integrated circuit processing, the importance of a number of issues has recently increased dramatically.

12.1.1 Resist Sensitivity

Because resist sensitivity directly affects process throughput, it is a fundamental consideration for the evaluation of resist process capability. In general, resist sensitivity can be shown to be proportional to thickness. For a direct photochemical (not chemically amplified), nonbleaching resist material, this is an exponential relationship determined by resist absorption and chemical quantum efficiency. However, as resist bleaching mechanisms are considered (as with the photochemical conversion of diazonapthoquinone to indene carboxylic acid), dynamic absorption exists, which introduces some additional considerations to this exponential decay. With chemically amplified resists, quantum efficiency is sufficiently high that the dependence of sensitivity on resist thickness becomes less of an issue and other considerations become of more concern.

12.1.2 Depth of Focus

The dependence of depth of focus on lens numerical aperture and wavelength can be exposed as:

$$\text{DOF} \quad \pm k_2 \frac{\lambda}{\text{NA}^2}, \tag{12.1}$$

where λ is wavelength, NA is numerical aperture, and k_2 is a process-dependent factor determined by process specification and requirement (a typical value for k_2 for a single-layer resist may be near 0.5, as shown in Chapter 11). As optical lithographic technology is pushed toward sub-200-mm wavelengths at numerical apertures greater than 0.6, DOF may fall below 0.5 μm. This presents an interesting challenge for substrate topography and photoresist thickness issues. With such a small useful DOF, and without the use of some method of planarization, it is not easy to predict exactly how large a fraction of this range could be consumed by photoresist thickness.

12.1.3 Limitations of Resist Aspect Ratio

The physical and chemical nature of a polymeric resist material will determine its limitations for high-aspect-ratio patterning. Additionally, the complex nature of development and process chemistry will influence limitations. As aspect ratio less than 3:1 is common for conventional single-layer resists. The limit to how fine the resolution can be for a single-layer resist of a given thickness is influenced to a large extent by polymer flow properties including glass transition temperature (T_g) and melting point (T_m). Because thermoplastic polymeric behavior is desired during processing, in which photoresist materials can go through cycles of heating, flowing, and cooling, they generally possess T_g values in the 70°C–180°C range. Materials of lower T_g will inherently be capable of lower-aspect-ratio imaging.

12.1.4 Reflection and Scattering Effects

Imaging over reflective substrates such as metal or polysilicon can allow significant intensity variation within a resist film. High levels of reflectivity may produce overexposure, manifested not only as a bulk effect over the entire imaged file, but also at pattern-specific locations such as line boundaries and corners. This is often referred to as *reflective line notching* or *necking*, which is a result of the scattering of radiation to unwanted field regions. Substrate reflection will affect the overexposure latitude and ultimately lead to a reduction in focal depth, limiting the amount of tolerable image degradation. To understand the impact of exposure latitude on depth of focus, consider imaging a feature with poor modulation. If a resist process is capable of resolving such a feature, it is likely to be possible only within a limited range of exposure dose. For a positive resist, overexposure can result in complete feature loss and underexposure can result in scumming. There is an intimate relationship, therefore, between depth of focus and exposure latitude. Decreasing the demands on focal depth increases exposure latitude. For a reflective substrate, if a large degree of overexposure latitude must be tolerated, the useful depth of focus will be reduced significantly. It is desirable to reduce any reflected contribution to exposure to eliminate feature distortion from scattering and to reduce detrimental effects on focal depth. This can be accomplished in a single-layer resist by several methods. First, because absorption is dependent on resist thickness, a thicker absorbing resist layer will decrease the impact of reflection. Other requirements drive resist toward thinner layers, however, reducing the practicality of this method. A second alternative is to increase the absorption of the resist so that little radiation is allowed to penetrate to the resist–substrate interface and then reflected back through the resist. The addition of dyes into a resist will accomplish this, but at the cost of resist-sidewall sensitivity, and resolution. The beneficial dynamic bleaching mechanism of the diazonaphthaquinone (DNQ)/novolac materials is undermined by the addition of an absorbing dye that makes no direct contribution to the photochemical process. An

alternative approach to reduction is the use of a multiplayer resist system, incorporating a separate antireflective layer.

12.1.5 Reflective Standing Wave Effects

An additional reflection phenomena that deserves consideration is the resist standing wave effect. This is an exposure variation within a resist layer resulting from coherent interference between incident and reflected radiation. The situation is described in detail in Chapter 2 and Chapter 9 and has significant impact on exposure, CD control, depth of focus, and coating uniformity requirements. Minimization of standing wave is generally desired. The addition of a resist dye can help reduce standing wave effect, but the impact on resist sidewall angle can be significant, as the top to bottom resist film attenuation increases.

12.1.6 Plasma-Etch Resistance

Postlithographic processing operations ultimately dictate the minimum acceptable resist thickness after development. For example, resist erosion during etch processing will increase any lithography-related thickness requirements. Furthermore, if new materials are considered for short wavelength exposure application, their etch resistance in halogen-based-plasma-etch processes may be reduced. Postlithographic processes may place the most restrictive demands on resist performance and may preclude any consideration of thinner single-layer resists.

12.1.7 Planarization

Because the lithography operations involved with integrated-circuit (IC) fabrication are rarely performed over a flat substrate, planarization of topography is a fundamental function of a resist material. The degree of planarization required for a specific level will be determined by step height, feature size and density, and substrate surface properties. Material properties of a resist, including polymer molecular weight, solids content, solvent type, coating-spin speed, acceleration, temperature, and exhaust will contribute to the extent of substrate smoothing. Polymeric materials with low molecular weight and a high solids content are generally employed for maximum results [1]. A fluid-dynamics approach can be used to demonstrate the relationships between process factors and planarization:

$$P \propto \frac{t\gamma h_0^3}{\eta w^4}, \tag{12.2}$$

where t is leveling time, γ is surface tension, h_0 is initial film thickness, η is solution viscosity, and w is feature width. This relationship suggests that several factors can be modified to

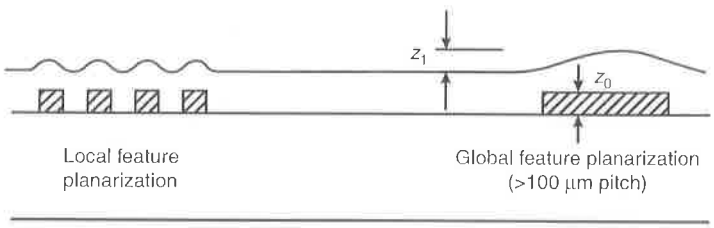

FIGURE 12.1
Polymeric planarization of local and global topography. The extent of planarization can be determined from measurement of initial and final step heights (z_0 and z_1).

affect net results. Planarization of close-proximity features (local geometry) and of widely spaced features (global geometry) may be required, depending on substrate characteristics and process needs. Figure 12.1 illustrates that planarization by a polymeric materials may be suitable for both situations. The extent of planarization can be quantified by considering the initially step height (z_0) and the final effective step height after smoothing (z_1) and determining the normalized ratio:

$$\text{Effective planarization} \quad \frac{z_0 \quad z_1}{z_0}, \tag{12.3}$$

which can be calculated for local and global features [2].

Planarization can be accomplished by means of substrate overcoating (generally with an organic polymeric film), etch-back processing, or polishing of topographic substrate to reduce step height. Techniques of chemical mechanical polishing (CMP) are becoming widely accepted alternatives to additive planarization methods, reducing constraints on resist processing and requirement for focal depth [3]. Methods of CMP can allow global planarization of both insulator and conductor layers in multilevel-metallization-interconnect structure and of both deep and shallow trench isolation materials. These techniques have become a critical path for both logic and memory production and a number of issues are receiving careful attention, including optimization of process techniques, cleaning considerations, and defects.

12.1.8 Multilayer Resist Processes as Alternatives to Conventional Resist Patterning

The appeal of multilayer resist processes and surface imaging resist (SIR) technology has increased because of the resolution enhancement they provide for the current optical exposure tools, as well as the potential application for new exposure systems such as 193-nm or extreme ultraviolet (EUV, 13–40 nm). At the shorter exposure wavelengths, conventionally developed resists are either unavailable or lack sufficient performance. With surface or near-surface imaging, photochemical modification necessary to affect the pattern transfer is restricted to a thin upper portion of the resist layer. Ideally, the imaging layer should be as thin and as planer as possible. In this way, maximum resolution can be obtained and optimum use can be made of the entire available focus range of the exposure tool. The resist image is free from the effects of device topography and substrate reflection, an advantage that becomes increasingly important as optical tools move to shorter wavelength sources, where the reflectivity of many materials increases. In addition, the high CD tolerances demanded by advanced IC designs require high-performance patterning, which multiplayer and surface imaging resisting systems can provide.

Multilayer techniques or single-layer SIR processes provide an advantage in application in which the substrate reflectivity is high or topography is severe. Patterning of DRAM gates, such as the one pictured in Figure 12.2, often provides such a challenging scenario. In this case, where 0.35-μm gates were patterned over 0.6 μm of topography, SIR techniques ensured constant CD control even over large step heights. Particularly in instances where the design dimensions challenge the resolution capability of the exposure tool and the resist, near-surface, or surface imaging techniques can play an important role.

A large number of polymeric multilayer systems have been developed and utilized over several decades. Multilayer schemes can be divided into four basic categories, with some overlap in function. Specifically, approaches have allowed planarization, reduction of reflection, contrast enhancement, and surface imaging. These categories are not

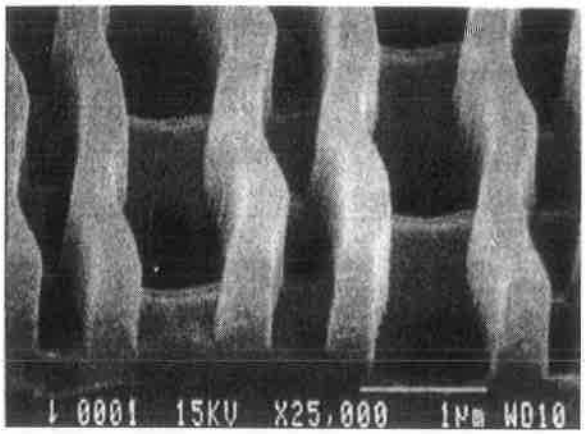

FIGURE 12.2
SEM micrograph of 0.35 μm DRAM gate structures patterned over 0.6 μm of topography using surface imaging techniques.

necessarily clearly divided, as a single multiplayer approach can accomplish several objectives. Details of these approaches will be explored in this chapter.

12.2 Multilayer Planarizing Processes—Wet Development Approaches

Various multilayer techniques have been introduced that employ polymeric planarization layers to reduce substrate topography and allow the use of a thin top-coated imaging resist layer, as depicted in Figure 12.3 [4]. Methods have included a wet-processed thick planarization layer [5], a two-layer portable conformable mask (PCM) [6], and a three-layer plasma transfer process [7]. The wet-processed approach leads to isotropic dissolution

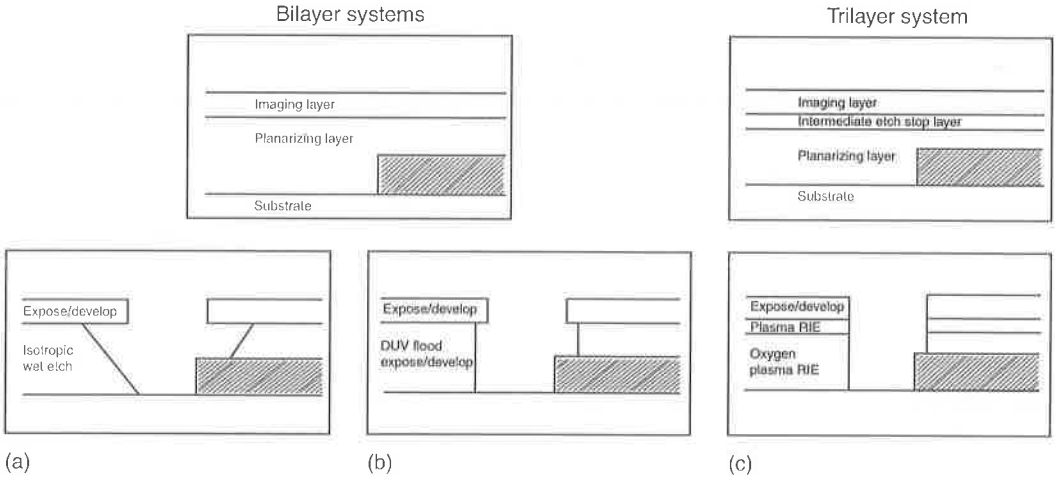

FIGURE 12.3
Multilayer approaches utilizing polymeric planarization layers. (a) A wet bilayer system using isotropic dissolution of the planarization layer; (b) a bilayer system with blanket deep ultraviolet (DUV) exposure of a photosensitive planarization layer masked by a patterned diazonaphthaquinone (DNQ)/novolac layer; (c) a typical trilayer resist system utilizing a planarizing layer, in etch stop layer, and an imaging layer.

of an underlying planarizing layer, limiting application generally to nonintegrated circuit use. The PCM process employs a deep ultraviolet (DUV)-sensitive planarizing layer, typically poly(methyl methacrylate), PMMA [8], or poly(dimethylgluterimide), PMGI [9], and a DNQ/novolac imaging layer. Because the DNQ/novolac is highly absorbing at wavelengths below 300 nm, once imaged it acts as a surface contact mask over the bottom resist layer. Deep ultraviolet flood exposure and development of the bottom layer allow pattern transfer through the entire multilayer stack. This technique can be limited by interfacial mixing of the two resist layers, which is minimized when using PMGI materials. Poor contrast of the DUV planarizing layer and reduced process control of this two-layer technique has limited resolution, making sub-0.5-μm imaging difficult.

Variations on the multiple-resist approach have also been used for electron beam T-gate fabrication [10,11]. Three resist layers may be used to allow specific feature shaping through the depth of a resist stack. For example, a bottom layer of PMMA is overcoated by a layer of a methyl methacrylate–methacrylic acid copolymer (PMMA–MAA), followed by a top coat of PMMA. Exposure and wet development lead to larger pattern widths in the more sensitive PMMA–MAA layer, allowing the formation of T-shaped metal gate structures through a subsequent additive liftoff process.

12.3 Wet-Development/Dry-Pattern Transfer Approaches to Multilayers

Anisotropic pattern transfer can allow significant improvement over the isotropic processing of wet-etched multilayer approaches. Through the use of a plasma-reactive-ion-etch (RIE) pattern transfer process, near anisotropy can be approached, allowing high-aspect ratio, fine-feature resolution [12,13]. The three-layer scheme, depicted in Figure 12.3, makes use of a polymeric planarizing layer (such as novolac resin or polyimide) and a thin intermediate etch-stop layer. This etch-stop layer can be a spin-on organosilicon compound (spin-on glass), a low-temperature oxide, a silicon oxinitride, or a metallic layer, which provide oxygen etch resistance. A thin resist imaging layer is coated over this etch-stop, exposed, and wet developed. Pattern transfer into the intermediate etch-stop layer can be achieved with wet-etch or dry-plasma techniques with suitable chemistry. Anisotropic pattern transfer through the thick polymeric planarizing layer can be achieved via an oxygen RIE process. Variations on this technique have been used for both optical and electron beam applications [14].

The importance of polymeric planarization approaches historically has declined as single-layer resists and CMP techniques have steadily improved. As shorter wavelength exposure technologies are pursued, however, it is likely that application of multilayer approaches will become more viable. A bilayer resist technique that allows planarization, etch resistance, and reflection control with a thin-imaging layer has many attractive properties. Such schemes will be addressed in detail as silicon-containing resists and top-surface imaging techniques are addressed.

12.4 Resist Reflectivity and Antireflective Coatings

Reflection at resist/substrate interfaces has been a concern for many IC generations. The impact is most pronounced when using high-contrast resists, a result of increasing exposure thresholding effects. Figure 12.4 shows the effect that varying resist film thickness has on feature size (CD swing curves) for an i-line resist imaged over polysilicon and

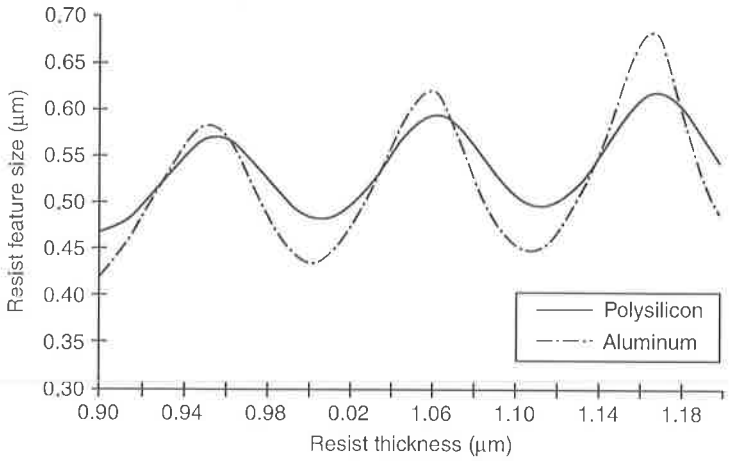

FIGURE 12.4
A critical dimension (CD) swing curve showing the effect of resist thickness variation on resist linewidth. Results for polysilicon and aluminum substrates are shown at 365 nm using a resist with a refractive index of 1.7.

aluminum films. The reflectance from a resist–polysilicon interface at 365 nm can be above 30% and, at 245 nm, above 38%. Resist over aluminum can produce reflectivity values of above 86% at 365 nm, and above 88% at 248 nm. Interface reflectance can be determined from a Fresnel relationship for two media at normal incidence as:

$$R \quad \left| \frac{n_2^* \quad n_1^*}{n_2^* + n_1^*} \right|^2. \tag{12.4}$$

Here, n^* is the complex refractive index or $n \quad ik$, where n is the real refractive index and k is the extinction coefficient. For nonabsorbing materials, $k \quad 0$ and $n^* \quad n$, simplifying Equation 12.4. For nonnormal incidence, an additional (cos θ) term is required, where θ is the angle of incidence. Inspection of the optical constants for materials in Table 12.1 gives an indication of the need to incorporate methods of reflectance control.

If the materials that make up the lithographic substrate possess low absorbance or are nonabsorbing, reflectance values at each interface must be uniquely considered to determine the net reflectance through the film stack. Figure 12.5 provides an example of a resist film over an SiO_2/Si substrate. Here, the contribution from the oxide–resist

TABLE 12.1
Optical Constants (n and k) for Several Materials at 436, 365, 248, and 193 nm

	193		248		365		436	
	n	k	n	k	n	k	n	k
Silicon	0.960	2.88	1.58	3.60	6.41	2.62	4.79	0.175
SiO_2	1.56	0.00	1.51	0.00	1.47	0.00	1.47	0.00
Si_3N_4	2.65	0.18	2.28	0.005	2.11	0.00	2.051	0.00
Aluminum	0.117	2.28	0.190	2.94	0.407	4.43	0.595	5.35
Polysilicon	0.970	2.10	1.69	2.76	3.90	2.66	4.46	1.60
Diazonaphthaquinone (DNQ)/novolac					1.70	0.007	1.67	0.007
PHS CAR			1.76	0.007				

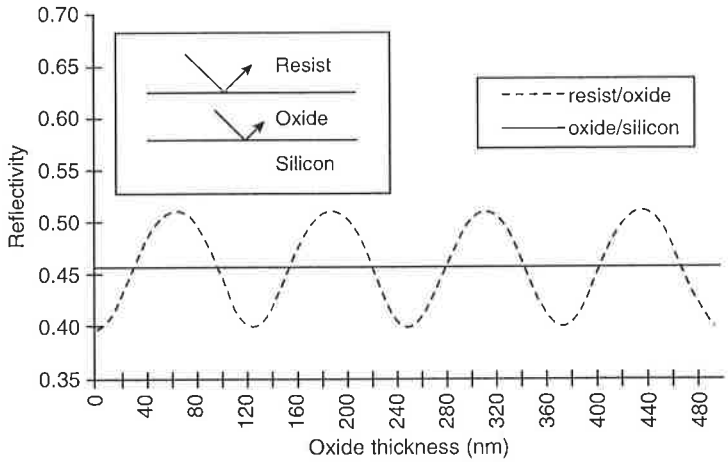

FIGURE 12.5
Reflection contribution at resist/oxide and oxide/silicon interfaces with increasing silicon dioxide thickness at a 365 nm wavelength using a resist with $n = 1.7$ and $k = 0.007$. Minimum reflectivity occurs at quarter wave oxide thicknesses.

interface is low compared with the contribution from the silicon underlying material. In this case, the thickness of the SiO_2 film can be adjusted to minimize total reflectivity through destructive interference (the use of quarter-wave approaches for inorganic antireflection materials will be discussed in detail in Section 12.4.1).

Control of reflectivity at the resist–substrate interface to values near a few percent is generally required for critical lithography levels, leading to the need for some method of control. The situation becomes more critical as lithographic methods incorporate shorter wavelength sources, a smaller spectral bandwidth, and more transparent resists. Reduction of reflection to values below 1% are needed for current generation lithography. Dye incorporation into a resist can reduce the coherent interference effects but at the cost of exposure throughput and sidewall angle, leading ultimately to resolution loss. Dyed resists are, therefore, generally limited to noncritical reflective levels, at which the highest resolution is not necessary.

Instead of reducing reflection effects through modification of a resist material, methods that reduce reflectivity at resist interface can provide control with minimal loss of resist performance. This can be accomplished through manipulation of thin-film optical properties and film thicknesses, and by careful matching of the optical properties of each layer in an entire resist/substrate stack.

12.4.1 Control of Reflectivity at the Resist–Substrate Interface: Bottom Antireflective Coatings

To reduce the reflectivity at the interface between a resist layer and a substrate, an intermediate film can be coated beneath the resist. This is known as a bottom antireflective coating (BARC). Inspection of Equation 12.4 suggests one approach where the refractive index of this layer could be close to that of the resist at the exposing wavelength. To reduce reflectivity, the film could then absorb radiation incident from the resist film. Thin-film absorption (α) is related to the optical extinction coefficient (k) as:

$$\alpha \quad \frac{4\pi k}{\lambda}, \tag{12.5}$$

and transmission through an absorbing film is

$$T \quad \exp(\ \alpha t), \tag{12.6}$$

where T is transmission and t is film thickness. A high extinction coefficient may therefore be desirable, leading to high absorption and low transmission through the BARC layer. As k is increased, however, reflectivity at the resist/BARC interface is also increased, as seen in Equation 12.4. An extinction coefficient value in the range of 0.25–1.25 may be reasonable, based on these considerations, and depending on resist material and film thickness demands. A series of plots showing substrate reflectance vs. BARC thickness for real-index matched materials with extinction coefficient values from 0.1 to 1.2 is shown in Figure 12.6. Because the BARC layer must accommodate pattern transfer (using either a wet or dry plasma etching approach), minimum thickness values are desirable. For these layer combinations, a BARC thickness between 500 and 800 produces a first reflectance minimum. These minima occur as reflectance from the BARC–substrate interface and interfere destructively with the reflection at the resist–BARC interface. This interference repeats at intervals of $\lambda/2n$ which can be explained by examining Figure 12.7. Here, radiation passes twice through the BARC layer with wavelength compression corresponding to its refractive index (λ/n_i). Two passes through a quarter-wave thickness ($\lambda/4n$) results in a half-wave phase shift directed toward the resist–BARC interface. This phase-shifted wave will then interfere with the reflected wave at the resist. Complete destruction will occur only if the amplitude values of the waves are identical, which is possible only if the reflectance at the resist–BARC interface is exactly equal to the reflectance at the BARC–substrate interface or if:

$$n_{\text{arc}} \quad \sqrt{n^*_{\text{resist}} \times n^*_{\text{substrate}}}, \tag{12.7}$$

This leads to a more complex route toward reflection reduction with a bottom ARC using both absorption and interference considerations.

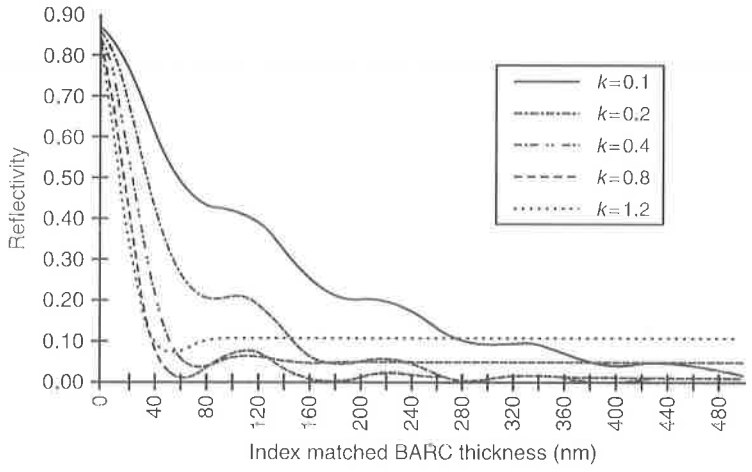

FIGURE 12.6
Substrate reflectivity vs. bottom antireflective coating (BARC) thickness for real index matched materials ($n = 1.7$ at 365 nm) and extinction coefficient values from 0.1 to 1.2. The best performance for a thin BARC layer may be possible with k values near 0.8.

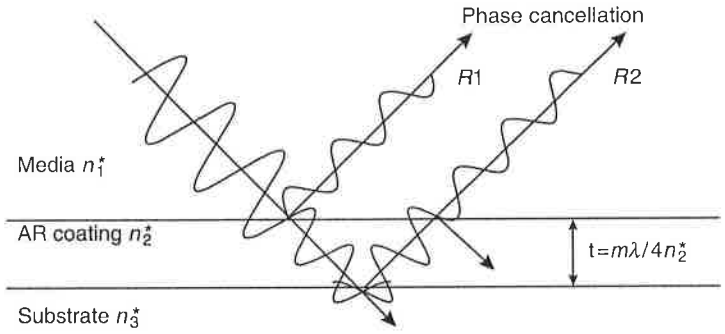

FIGURE 12.7
Diagram of the principle of a quarter wave antireflective (AR) layer between two media. A thickness of the AR coating is chosen to produce destructive interference between reflected components, R_1 and R_2. The ideal refrac tive index is $\sqrt{n_1^* n_3^*}$.

Reflection control and aspect ratio requirements need to be considered to determine optimum ARC film thickness values. A first reflectance minimum corresponding to a relatively thin film may be chosen for fine feature pattern transfer. If thicker layers can be tolerated, further reduction in reflectivity may be achieved by increasing the BAC film thickness. There is an exponential trend in reflection reduction with increasing thickness and BARC absorption. As extinction coefficient values increase toward 0.8, reflection begins to increase, and for values above 1.2, reflectivity below a few percentage becomes difficult. Figure 12.8 and Figure 12.9 are a series of contour plots of substrate reflectivity for BARC films with extinction coefficient values from 0.0 to 0.9 and refractive index values from 1.8 to 2.7.

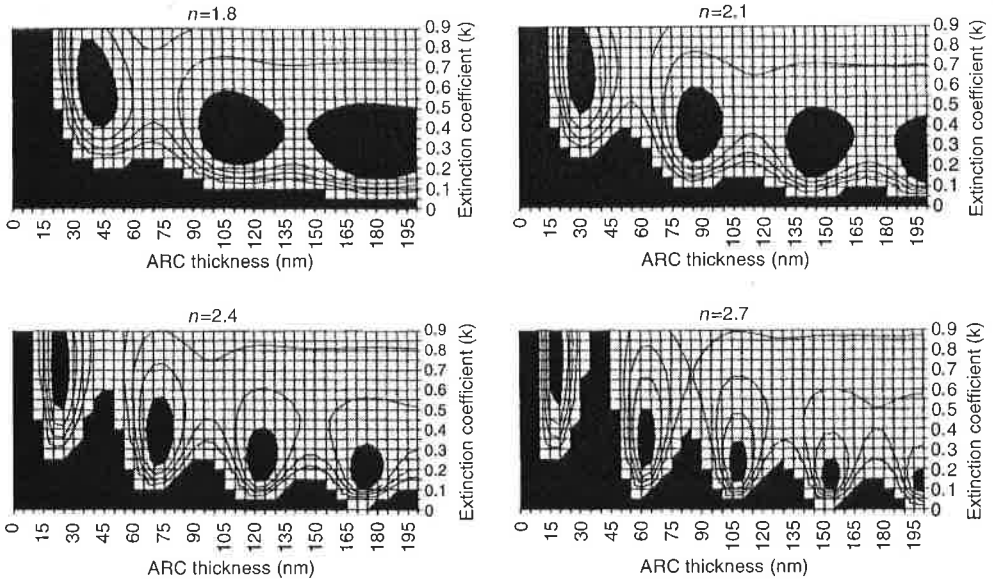

FIGURE 12.8
Contour plots of substrate reflectivity (over silicon) at 248 nm as a function of bottom antireflective coating (BARC) thickness for materials with refractive indices between 1.8 and 2.7 and extinction coefficient values to 0.9. Central contour areas correspond to 0 2% reflectivity and 2% constant contours are shown. Results beyond 10% reflectivity are shown in black [$n_{\text{resist}}(248) = 1.75$].

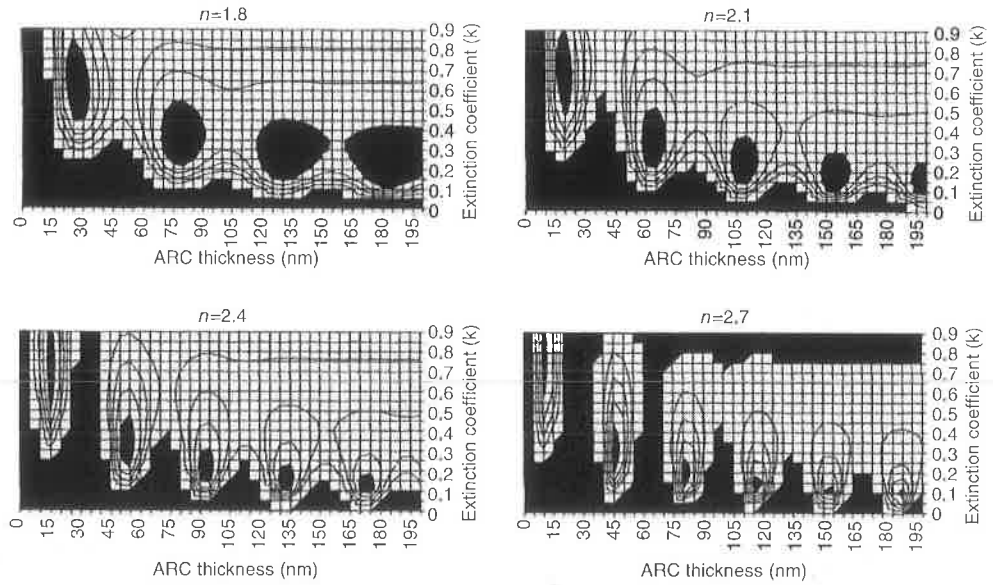

FIGURE 12.9
Contour plots of substrate reflectivity (over silicon) at 193 nm as a function of bottom antireflective coating (BARC) thickness for materials with refractive indices between 1.8 and 2.7 and extinction coefficient values to 0.9. Central contour areas correspond to 0 2% reflectivity and 2% constant contours are shown. Results beyond 10% reflectivity are shown in black. Resist refractive index is 1.6.

12.4.1.1 Organic BARCs

Organic BARC materials have been used for some time, typically in the form of spin-on polymeric materials [15]. These polymers contain highly absorbing dyes introduced at levels to deliver appropriate extinction coefficient values. Several classes of materials can be used, depending to a large extent on the pattern transfer requirements of a process [16–19]. Wet developable organic BARCs based on partially cured polyamic acids (polyimide precursors) have been utilized for large feature geometry. These materials, with refractive index values near 1.7 and extinction coefficients near 0.3, are coated and partially cured prior to resist application. Partial curing of the dyed polyamic acid allows tailoring of the alkaline solubility of the layer to match that of exposed resist. Bottom antireflective coating materials made of dyed triazine derivatives have also been introduced [17].

As shown in Figure 12.10, exposure and development of an aqueous base-soluble resist layer exposes the underlying BARC material, which is also base-soluble if cured appropriately. Materials have been formulated that provide a high degree of bake latitude (as high as +20°C) [20] and exhibit a very low degree of interfacial mixing. The inherent problem with this approach for antireflection is the isotropy of wet pattern transfer. With no preferential direction for etching, undercutting results to the full extent of the BARC thickness. As shown in Figure 12.10, resist features are undercut by twice the BARC thickness, limiting application of wet-developed organic materials to a resolution above 0.5 μm.

Dry-etch-compatible organic BARC materials can allow control of the etch profile through use of plasma RIE methods of pattern transfer. The requirements then become one of resist to BARC etch selectivity to minimize resist erosion and the accompanying loss in process and CD control. Initial candidate materials for use as dry etch BARCs may be polymers that undergo efficient scissioning with plasma exposure, leading to increased

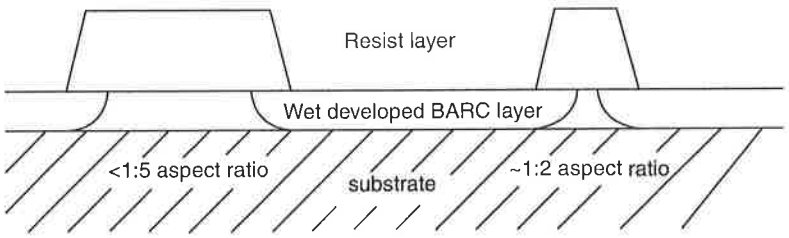

FIGURE 12.10
Process schematic for an aqueous base developed bottom antireflective coating (BARC). Exposure and development of a top resist layer allow development to continue through a suitably baked AR film. Isotropic pattern transfer limits this approach.

volatility. For instance, dyed polyolefin sulfone materials (frequently employed as electron beam resists) [21] could allow relatively high oxygen-based RIE etch selectivity to novolac or polyhydroxystyrene (PHS) resist materials. Several dry-etch materials have been introduced [22,23] for use in 248-nm and i-line application. Figure 12.11 shows lithographic results and reduction of reflective standing wave effects with use of a dry-etch BARC material.

A potential problem with spin-on organic BARC materials is their planarizing nature. As seen in Figure 12.8 and Figure 12.9, control of film thickness to a few tens of angstroms may be required for suppression of substrate reflectivity. If a polymeric material is spin-coated over severe topography, film thickness can deviate substantially from a targeted value. The film is generally not conformal, which leads to significant variation in reflection reduction across a field. To increase the conformal properties of a BARC layer, alternative deposition methods can be explored. Also, through elimination of the polymeric nature of the BARC material, planarization can be further reduced. This leads to a class of inorganic antireflective materials that can be coated using chemical vapor or vacuum deposition methods.

12.4.1.2 Inorganic BARCS

Vapor-deposited ARC materials were first proposed for use over aluminum [24] and have since been applied over a variety of reflective substrate layers. The optical requirements for an inorganic layer are generally the same as for organic films. This is, however, a more difficult task with inorganic dielectric materials than it is with organic polymers as practical material choices are generally limited to those that allow process compatibility. The challenges for organic and inorganic materials can therefore differ. For inorganic

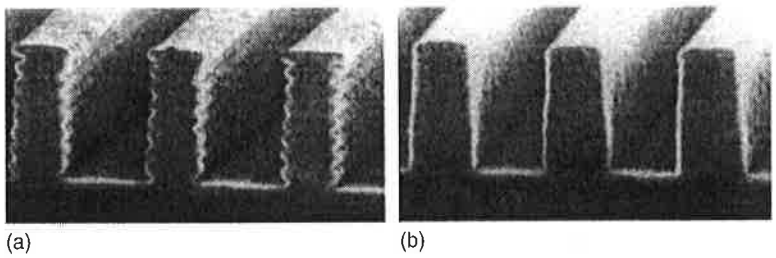

FIGURE 12.11
Comparison of reflective standing wave reduction through use of a dry etch bottom antireflective coating (BARC): (a) without a bottom ARC; (b) with a bottom ARC.

films, the flexibility of optical constants is made possibly to some extent through material selection and variation in stoichiometry. Deposition thickness and uniformity can be controlled accurately to the nanometer level, and films generally conform to the underlying topography. The choice between inorganic or organic BARC materials, therefore, depends in part on the underlying substrate and processing that will be encountered. Titanium nitride [25], silicon nitride, silicon oxinitride [26], amorphous carbon [27], tantalum silicide [28], and titanium tungsten oxide [29] films have been used as inorganic antireflection layers at 365, 248, and 193 nm [30]. Substrate-resist interaction effects for 248-nm chemically amplified resists also need to be considered as candidates are evaluated, which may reduce the attractiveness of some materials for some ARC applications [31].

For nonstoichiometric materials such as silicon oxinitride, modifications in stoichiometry can be used to tailor optical properties. Traditionally, a chemical compound is thought of as having a fixed atomic ratio and composition. A wider range of properties is possible by relaxing this stoichiometric requirement. By controlling the ratios of material components during deposition, optical behavior can be modified. It is not immediately obvious that nonstoichiometric composite films of metal, insulator, or semiconductor combinations will exhibit predictable optical properties. Through analysis of the atomistic structure of materials, and by relating optical material properties to electrical properties, some conclusions can be drawn [32]. Optical constants can be related to electrical properties by neglecting material structure and considering macroscopic material quantities only:

$$n^2 \quad \frac{1}{2}\left(\sqrt{\varepsilon_1^2 + \varepsilon_2^2} + \varepsilon_1\right), \tag{12.8}$$

$$k^2 \quad \frac{1}{2}\left(\sqrt{\varepsilon_1^2 + \varepsilon_2^2} \quad \varepsilon_1\right), \tag{12.9}$$

where ε_1 and ε_2 are real and imaginary dielectric constants, respectively. To account for material structure, Drude analysis of optical and electrical constants describes free electron or metallic behavior quite well in the visible and infrared (IR) region [33]. Equation 12.10 and Equation 12.11 are Drude equations for optical and electrical constants, related to material plasma frequency (ν_1) and damping frequency (ν_2):

$$n^2 \quad k^2 \quad \varepsilon_1 \quad 1 \quad \frac{\nu_1^2}{\nu^2 + \nu_2^2}, \tag{12.10}$$

$$2nk \quad \varepsilon_2 \quad \left(\frac{\nu_2}{\nu}\right)\frac{\nu_1^2}{\nu^2 + \nu_2^2}. \tag{12.11}$$

To account for optical properties at shorter wavelengths, bound-electron theory needs to be utilized. For dielectric materials, no intraband transitions exist because of filled valence bands. Interband transitions are also limited in IR and visible regions because of large band gap energies. Bound-electron theory alone is sufficient to describe classical dielectric behavior. Characterization of metallic and noninsulating materials in UV and visible regions requires use of both free-electron and bound-electron theory. By assuming a given number of free electrons and a given number of harmonic oscillators, optical properties over a wide wavelength range can be described. Using bound-electron or harmonic-oscillator theory, relationships for optical and electrical constants can be

determined from the following equations:

$$\varepsilon_1 \quad 1 + \frac{4\pi e^2 m N_a (\nu_0^2 \quad \nu^2)}{4\pi^2 m^2 (\nu_0^2 \quad \nu^2)^2 + \gamma' \nu^2}, \tag{12.12}$$

$$\varepsilon_2 \quad \frac{2e^2 N_a \gamma' \nu}{4\pi^2 m^2 (\nu_0^2 \quad \nu^2)^2 + \gamma' \nu^2}, \tag{12.13}$$

where γ is the damping factor, N_a is the number of oscillators, m is electron mass, and e is electron charge. From this analysis, it can be shown that the optical properties of a material can be described by metallic behavior combined with dielectric behavior. Figure 12.12 shows plots of optical constants for a metallic film using the Drude model for free-electron motion and metallic-dielectric composite films using combined free- and bound-electron models. These results suggest that the optical properties of a composite material can be modified by controlling the ratio of its components. It is expected, therefore, that the optical properties of nonstoichiometric materials would fall somewhere between those of their stoichiometric elemental or compound constituents.

Silicon nitride (Si_3N_4) possesses optical constants that may be a good starting point for use as an ARC at several wavelengths. Optical constant data for silicon nitride, silicon dioxide (SiO_2), and silicon at 436, 365, 248, and 193 nm are contained in Table 12.1 [34]. By adjusting the deposition parameters during film formation (gas flow ratios for CVD and power, pressure, and gas flow for sputtering, for instance), thin-film materials can be produced with optical properties defined by these constituents. Figure 12.13 shows the reflectivity at the substrate interface for several 248-nm SiON ARC materials under a resist with a refractive index of 1.76. Shown also in Figure 12.14 are the optical constants (n and k) for a variety of materials at 193 nm [35]. From these data, together with compatibility and process requirements, potential ARC films for 193 nm can also be identified.

An additional advantage from the use of inorganic ARCs is the ability to grade the indices of materials to best match requirements of resist and substrate layers [36]. This is possible through control of process parameters during deposition. To achieve similar results with organic spin-on ARCs, multiple layers would be required. Pattern transfer for inorganic antireflective layers can also result in higher selectivity to resist, made possible, for instance, if fluorine-based etch chemistries are used. Shown in Figure 12.15 is a comparison of pattern transfer processes through an organic spin-on ARC and an

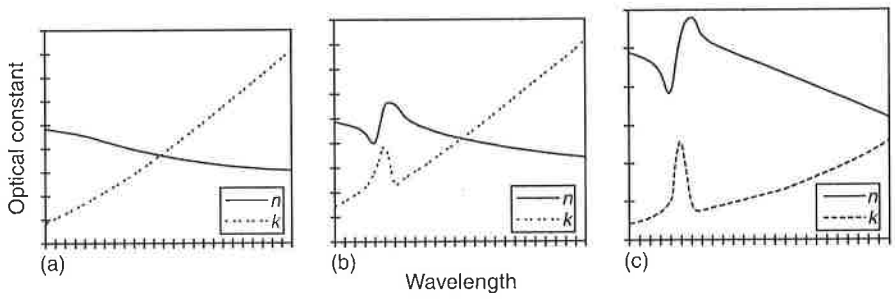

FIGURE 12.12
Plots of optical constants for a metallic film using the Drude model for free electron motion and metallic dielectric composite films using combined free and bound electron models. (a) A metallic film; (b) a dielectric film; and (c) a dielectric composite film with increasing metallic content.

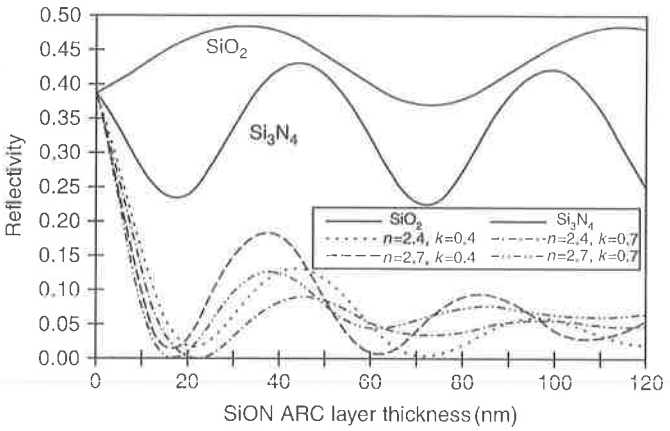

FIGURE 12.13
Reflectivity at the resist/substrate interface for several 248 nm understoichiometric SiON antireflective coating (ARC) materials under a resist with a refractive index of 1.76. The underlying substrate is polysilicon. Reflectivity for stoichiometric SiO_2 and Si_3N_4 are also shown.

inorganic ARC with high resist selectivity [37]. Minimum resist erosion during the etch process with the inorganic material can result in an increase in CD control. A major compromise when using inorganic materials is the increased complexity of deposition processes over spin coating. Process trends and requirements will probably lead to incorporation of both approaches for various lithographic operations.

12.4.2 Top Antireflective Approaches

The bottom antireflective approach leads to reflection reduction at the interface between a resist material and the substrate. Reflection also occurs at the top of the resist, at the resist–air interface, as shown in Figure 12.16. This leads to a situation similar to that of a Fabry–Perot etalon. An expression for the reflective swing ratio can be utilized to address

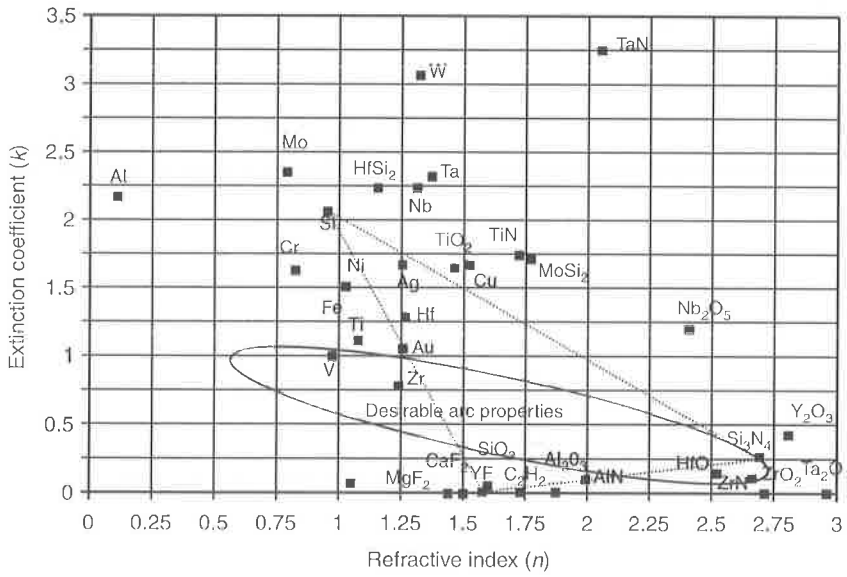

FIGURE 12.14
A plot of the optical constants (n and k) for various materials at 193 nm. A window of desirable antireflective coating (ARC) properties is shown, as also described in Figure 12.9. An understoichiometric SiON film would also suffice for use at 193 nm, with properties falling within the area defined by dashed lines.

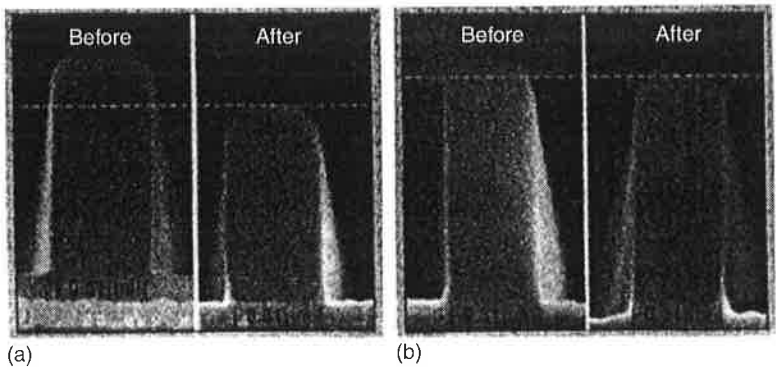

FIGURE 12.15
A comparison of resist loss during pattern transfer to bottom ARC layers. (a) Organic spin on ARC; and (b) dielectric inorganic ARC. (From Bencher, C., Ngai, C., Roman, B., Lian, S., and Vuong, T. *Solid State Technology*, 111, 1997.)

reflection effects within an entire resist film stack [38]:

$$\text{Swing} \quad 4\sqrt{R_1 R_2}\exp(-\alpha t), \tag{12.14}$$

where R_1 is the reflectivity at the resist–air interface, R_2 is the reflection at the resist–substrate interface, α is resist absorbance, and t is resist thickness. Here, the swing is the ratio of the peak-to-valley change in intensity to the average intensity, which is desired to be a minimum. A decrease in R_2 via a BARC layer can be used to accomplish this, as can an increase in absorption (through use of a resist dye, for instance) or an increase in resist thickness. A reduction in R_1 is also desirable and can be addressed through the use of a top antireflective coating (TARC) [39]. Because there is a mismatch between refractive indices of the resist material and air, R_1 can be on the order of 7%. This can lead to resist exposure and CD control problems, encountered as a result of internal reflectance via multiple interference effects, scattered light, and reflective standing wave. An exposure-tool alignment signal detection can also be degraded from top surface reflection effects [40]. Like conventional AR coatings for optical applications, TARC films are not absorbing materials but instead transparent thin-film interference layers that utilize destructive interference to eliminate reflectance. The ideal refractive index for such a film coated over a resist material

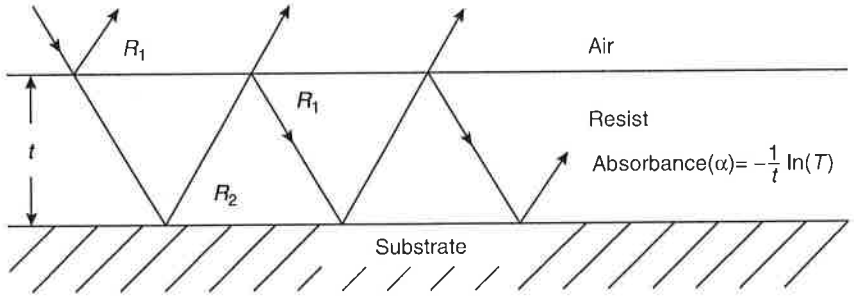

FIGURE 12.16
Diagram of reflection contribution from resist/substrate and resist/air interfaces.

is that which produces equivalent reflectance from the air and from the resist side of the interface. This leads to an optimum index of

$$n^*_{AR} \quad \sqrt{n^*_{air} \times n^*_{resist}}. \tag{12.15}$$

If a film of this index is coated to a quarter-wave thickness ($\lambda/4n_{ARC}$), complete destructive interference can occur. For i-line resist materials with a refractive index of 1.70, an ideal TARC material would have an index of 1.30 and would be coated at 700 Å. Figure 12.17 shows the reduction in reflection for a quarter-wave top AR layer when the refractive index is varied from 1.1 to 1.5. For refractive index values below 1.3, there is a larger contribution to reflection from the resist–TARC interface. At values above 1.3, the contribution from the air–TARC interface is larger.

The refractive index and reflectance properties of several TARC materials are given in Table 12.2. As the refractive index of a material approaches the ideal value of $\sqrt{n^*_{air} \times n^*_{resist}}$, the reflectances at the resist and air interfaces are equivalent, allowing destructive interference at a quarter-wave thickness. Residual reflectances result as TARC indices deviate from the ideal. To achieve refractive index values near the ideal 1.3, polyfluoroalkylpolyethers and polytetrafluoroethylene-based materials cast in solvents that do not dissolve novolac resist materials have been utilized at TARC layers [41,42]. These fluorinated polymers require removal with chlorofluorocarbons prior to development and have been replaced by water-based and water-soluble materials to improve process compatibility [43]. Although these materials do not possess a refractive index as close to the ideal values for use with DNQ/novolac resists at 436 and 365 nm (the refractive index is 1.41 at 365 nm), the reduced process complexity makes them a more attractive choice over solvent-based systems. Figure 12.18 shows the reflectivity of a resist film stack as resist film thickness is varied. Reflectivity varies by over 20% for resist over polysilicon over one swing period. This is reduced significantly with the addition of a water-soluble TAR coated to a quarter-wave thickness. Exposure and focus-latitude improvement has also been demonstrated with these materials.

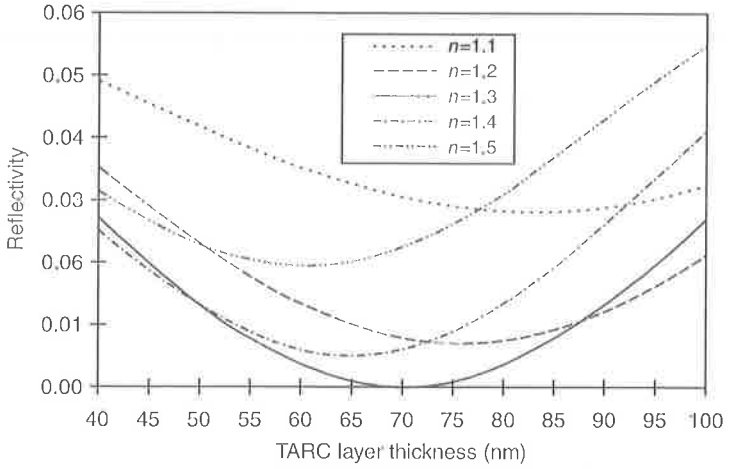

FIGURE 12.17
The reduction in surface reflection through use of a top antireflective coating (TARC) material at 365 nm. Reflection can be eliminated through use of a quarter wave thickness (700 Å) of a material with a refractive index of 1.3.

TABLE 12.2

Refractive Index and Reflectance Properties of Several Top Antireflective Coating (TARC) Candidates

	Refractive Index, n (365 nm)	Departure from Ideal	Quarter Wave Thickness at 365 nm	Reflectance at Air Interface	Reflectance at Resist Interface
Polyvinyl alcohol	1.52	0.32	600 Å	4.26%	0.3%
Polyethylvinylether	1.46	0.16	625 Å	3.5%	0.6%
Polyfluoroalkylpolyether	1.27	0.02	713 Å	1.5%	2.0%
Aquatar [12]	1.41	0.11	647 Å	2.9%	0.9%
Ideal[a]	1.30		702 Å	1.8%	1.8%

[a] Assuming a resist refractive index of 1.70.

12.5 The Impact of Numerical Aperture on Reflectance Effects

In Equation 12.4 and Equation 12.14, the assumption of normal incidence is made. In projection imaging, the incident angle of illumination is a function of the NA of the optical system. Reflectance at an interface is a function of the angle of incidence (in air) I_1 and the angle of refraction I_2 as

$$R \quad \frac{1}{2}\left[\frac{\sin^2(I_1 \quad I_2)}{\sin^2(I_1 + I_2)} + \frac{\tan^2(I_1 \quad I_2)}{\tan^2(I_1 + I_2)}\right]. \tag{12.16}$$

The first term in this equation corresponds to the reflection that is polarized in the plane of incidence and the second term corresponds to the reflection in the perpendicular plane. The effective film thicknesses for resist, AR layers, and underlying dielectric films are also

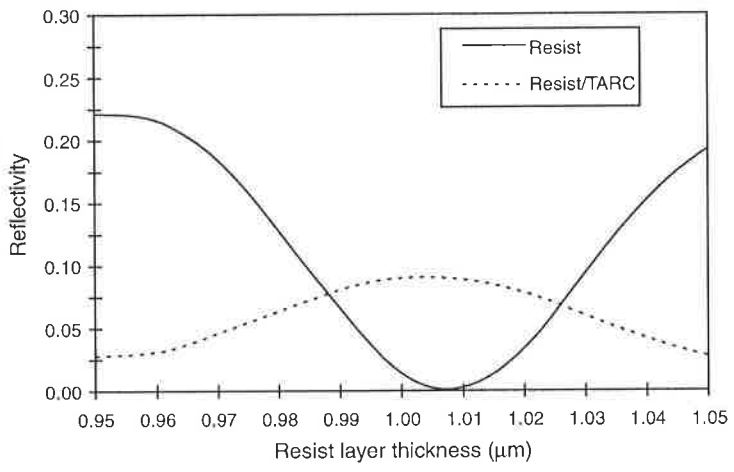

FIGURE 12.18
Reflective at the top surface of a resist material as a function of resist thickness with and without a top antire flective coating (TARC). Results are for 365 nm and a polysilicon substrate. The refractive index of the TARC is 1.41 and its thickness is 647 Å.

scaled by the angle of incidence as ($t \cos \theta$), where t is the thickness of the film at normal incidence. Large angles of incidence (with high-NA optics) have been shown to contribute to reducing the reflective swing ratio [44].

12.6 Contrast Enhancement Materials

Resolution is generally limited in optical lithographic processes by the inability of a resist material to adequately utilize a degraded aerial image. Optical improvement techniques including the use of lenses with a higher numerical aperture, shorter wavelength exposure sources, modified illumination, or phase shift masks can be employed to improve aerial-image integrity through a sufficiently large focus depth. Additionally, the use of a thinner, higher contrast resist over a low-reflective substrate can best record aerial images of limited modulation. The concept of a contrast enhancement material (CEM) coated over a resist allows an alternative to these approaches, making use of an intermediate image capture step prior to image transfer into photoresist. Contrast enhancement is based on the use of photobleachable materials that are opaque prior to exposure, but become transparent after photoabsorption [45–47]. The process is illustrated in Figure 12.19. Here, an aerial image of low modulation is incident on a thin CEM layer coated over resist. During exposure of the CEM, its transparency increases until the resist interface is reached, at which time resist exposure begins. If the dynamic photobleaching rate of the CEM is low compared with the exposure rate of the underlying resist, the CEM image becomes an effective contact masking layer. This masking layer transfers the image into the underlying resist. The net effect is to increase the effective contrast of the resist process.

To be applicable for a microlithographic process, CEM materials must exhibit optical absorbance values above 2 at thicknesses on the order of minimum feature sizes. Figure 12.20 shows the spectral characteristic of a 365-nm water-soluble material consisting of an inert polymer film and an organic dye. Upon exposure, photoisomerism of the organic dye increases transparency near 365 nm. Several materials have also been introduced for exposure wavelengths of 436, 365, and 248 nm [48–50].

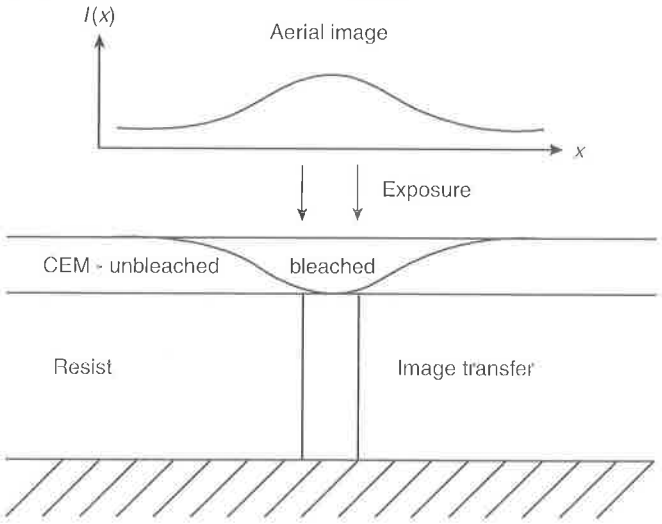

FIGURE 12.19
Schematic of a photobleachable contrast enhancement material (CEM) process. The CEM material acts as a contact mask for exposure of an underlying resist.

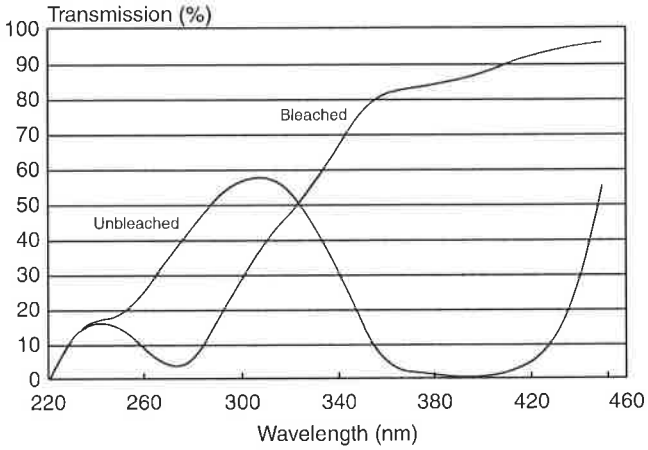

FIGURE 12.20
Transmission characteristics of a water soluble contrast enhancement material (CEM) for use at 365 nm.

12.7 Silicon-Containing Resists for Multilayer and Surface Imaging Resist Applications

Multilayer resist techniques have long been used to ease requirements for resist performance [51–56]. This goal is achieved by using physically distinct layers to separate the imaging function from the etch resistance, planarization, and reflection suppression function. Trilevel resists have demonstrated enhanced resolution compared with single-layer resist processing. The trade-off for this resolution, however, is additional processing difficulty as the deposition and patterning of three layers must now be simultaneously controlled. Although excellent results have been obtained, the processing complexity has been the major obstacle for the widespread application to production of integrated circuits.

An obvious simplification of the original multilayer technique is to incorporate the patterning and etch resistance into one layer and require only one additional layer for planarization. Eliminating the middle layer requires that the top layer have sufficient etch resistance and that there are no detrimental interactions between the top and bottom resist layers. The use of resists containing organosilicon and organometallic polymers on top of a thick organic planarizing layer has been reported [57]. The top resist layer is developed using standard wet development techniques and the image is transferred to the bottom resist layer with an oxygen-plasma etch. A refractory oxide, which is highly etch resistant, is formed in the top resist layer during the oxygen plasma etch [58,59]. Taylor et al. [60,61] demonstrated the selective introduction of silicon into the resist polymer following exposure of the resist. During the oxygen-plasma development, a protective SiO_2 coating is formed on the polymer surface that is resistant to etching [62].

12.7.1 Bilayer Process with Silicon-Containing Resists

Silicon-containing resists for use in bilayer imaging processes are an ideal choice because of the compatibility with silicon semiconductor processing [63–65]. Many variants of silicon-containing polymers for use in resists were developed; however, early polymers required organic solvents for development and did not possess either sufficient resolution or sensitivity [66,67]. Addition of fluorescence quenches improved the photosensitivity for polysilanes by a factor of 5, although development of the sub-0.5-mm features patterned

with a 0.35 NA, 248-nm stepper was still performed in an organic solvent [68]. For aqueous development of silicon-containing resists, loss of resolution is often observed because the silicon-containing groups that are incorporated in the resists interfere with the development process by significantly altering the resist hydrophilicity.

Silicon-containing bilayer resists have received renewed attention for use at an exposure wavelength of 193 nm. A silicon-containing bilayer process capable of imaging 0.175-nm equal lines and spaces with a 193-nm, 0.5 NA stepper has been demonstrated [69]. This silicon-enriched methacrylate-based top imaging layer can be developed in standard tetramethylammonium hydroxide solution. Interestingly, the top imaging layer is relatively thick (2500 Å), suggesting that even finer resolution could be achieved if a thinner imaging layer could be used.

12.7.1.1 Silicon Chemical Amplification of Resist Lines Process

A variation of the silicon-containing bilayer scheme known as Si-CARL (silicon chemical amplification of resist lines) [70,71] is illustrated in Figure 12.21. Silicon chemical amplification of resist lines is a typical bilayer process in that a thin imaging layer is applied on top of a thick planarizing layer. A strongly crosslinked novolac resist film of sufficient thickness to suppress substrate reflections and standing waves is used as the bottom layer. The top resist contains an anhydride, which is converted via acid-catalyzed hydrolysis to a soluble carboxylic acid. The Si-CARL process incorporates silicon into the resist after the top film has been exposed and developed. An amino-containing siloxane such as bis-diaminoalkyl-oligo-dimethylsiloxane reacts chemically with the anhydride and provides the etch resistance for the top resist layer during the subsequent plasma etching of the bottom layer.

The silicon incorporation in the Si-CARL process is typically performed in solution using conventional track equipment, but the dry development step is carried out using a plasma reactor. The bifunctional oligomers used for silicon delivery, so-called *CARL reagents*, have a reactive amine group at each end of the chain and incorporate multiple

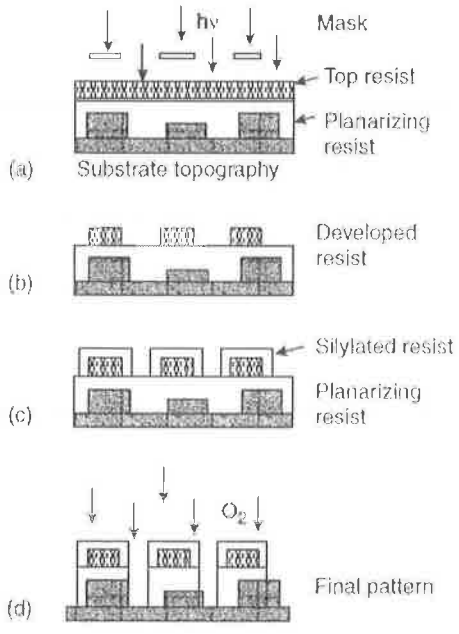

FIGURE 12.21
Illustration of the silicon chemical amplification of resist lines (Si CARL) process. (a) Exposure of top resist; (b) aqueous development of top layer; (c) silylation of top pattern resulting in linewidth increase; (d) dry etch transfer of image to bottom layer.

silicon atoms at each binding site in the resist polymer. These diamines can also react with different polymer chains to cause crosslinking in the resist polymer. A very high silicon content in the resist, up to 20%–30% (by weight), can be achieved. After inclusion of these oligomers, the additional organic material incorporated in the resist is responsible for the swelling (i.e., amplification) of the original resist pattern. This increase in film thickness is reportedly linear in silylation time and does not appear to be inhibited by increasing crosslinking. In addition, the corresponding line with increase is independent of feature size [72]. Depending on the time during which the resist is exposed to the CARL reagent, the resulting pattern can be either the same size as the mask dimensions or the space can be reduced beyond the design size. Thus, depending on dose and aqueous silylation time, it is possible to introduce a process bias to pattern subresolution spaces. Interestingly, no observed pattern deformation or distortion has been reported with this process [72]. It is important to note that in the Si-CARL process the entire surface of the developed resist feature incorporates silicon and therefore is resistant to sizing changes during the plasma patterning of the bottom layer of resist. Very high aspect ratio patterns have been demonstrated with these methods [70].

A top surface imaging variant of this process, called simply *top-CARL*, can be implemented as a single-layer process in which exposure to the CARL reagents and selective silicon uptake occur in the exposed area before development has taken place [70]. However, the Si-CARL bilayer process has a larger process latitude and greater etch resistance. Changes in the photoactive compound and matrix resin have been used to tailor the CARL and Si-CARL process for g-line, i-line, 248-nm, 193-nm lithography, and e-beam lithography. Both positive and negative tone systems have been developed [73].

The Si-CARL process has the advantages of a bilayer technique (topographic invariance, reflection suppression, enhanced resolution) and can allow the optical exposure tools to operate in a more linear sizing regime. This can be advantageous for levels such as contacts, which are notoriously difficult to pattern. Another advantage of the Si-CARL process is the use of an aqueous-based, room temperature silylation scheme that can be performed on a conventional resist development track.

12.7.1.2 Other Bilayer Techniques Involving Silicon Incorporation

The silicon-added bilayer resist on SABRE process [74] is very similar to the Si-CARL technique except that silicon is introduced into the patterned top layer using a gas-phase process. In the SABRE process, conventional novolac-based g-line resists are silylated using bifunctional silylating agents to prevent resist flow and deformation. A major drawback of the SABRE process is that the silicon incorporation step is extremely slow, reportedly requiring 5–90 min, depending on the silylating agent [74].

The difficulties in formulating a single-layer resist with sufficient transparency and etch selectivity for patterning at 193 nm and even shorter wavelengths have intensified investigations of various bilayer schemes, particularly those involving introduction of silicon into the resist after it has been exposed. A bilayer approach has been demonstrated that incorporates silicon after exposure of the top resist layer by DUV (248 nm) or extreme ultraviolet (EUV; 13.5 nm) wavelengths [75,76]. As illustrated in Figure 12.22, crosslinking induced by the photogenerated acid and the subsequent postexposure bake provides differential silicon permeability in the exposed and unexposed areas of the imaging layer. Silicon is preferentially incorporated in the unexposed resist from a gas-phase reagent after the exposure and bake steps. As with the Si-CARL process, some increase in resist volume accompanies the silicon incorporation. Further

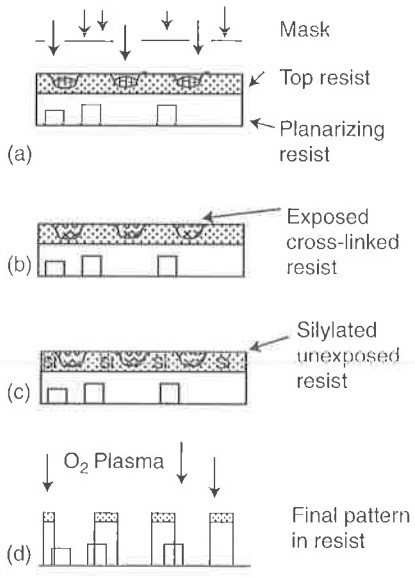

FIGURE 12.22
A silylated bilayer approach for using chemically amplified resists. (a) Exposure and generation of photoacid; (b) postexposure bake and crosslinking of exposed resist; (c) silicon incorporation into unexposed resist; and (d) dry etch transfer of image.

improvements in the process are achieved by introducing small amount of a difunctional disilane to control the resist swelling and to improve both the selectivity of the silicon inclusion step and process resolution [75]. Exposure to an oxygen-containing plasma for the all dry development step produces an etch resist silicon oxide mask in the unexposed regions resulting in a positive tone pattern.

The silylated bilayer system depicted in Figure 12.22 employs chemical amplification, which, because of the low exposure dose requirements, is compatible with the limitations for the present 193-nm and EUV exposure tools. The difficulty with these systems is providing sufficient silicon incorporation into the resist, while maintaining adequate contrast between the exposed and unexposed portion of the resist [76].

The use of unique materials as top imaging layers is also being explored. For instance, a bilayer process has been developed in which an imaging layer is formed by plasma-enhanced chemical vapor deposition (PECVD) from tetra-methylsilane deposited on a PECVD planarizing layer. The PECVD process allows a very thin conformal top imaging layer to be applied [77].

Although the bilayer processes show some of the advantages of surface imaging, they are limited primarily by process complexity. Not only two separate resist applications are necessary, but also in most schemes both conventional wet development and dry development equipment are needed. This complexity generally translates into higher final costs that have kept many systems from becoming widely adopted. Defect and particle generation and problems with pinholes in the top imaging and barrier layers are additional problems with multilayer techniques [78,79]. With the notable exception of the Si-CARL and CARL processes, bilayer approaches are generally viewed as a method for extending the exposure tool capability and for research applications but not as manufacturable processes.

12.8 Silylation-Based Processes for Surface Imaging

Instead of applying two distinct layers for patterning, the concept of selectively incorporating an inorganic or organometallic substance into either the exposed or unexposed

regions of a single resist layer was demonstrated by Taylor et al. [60,61]. Effectively, silicon-containing bilayer was achieved post patterning by the reaction of $SiCl_4$ with the photochemically altered resist, a process termed gas-phase functionalization. In a similar vein, MacDonald et al. [80,81] used photogenerated OH reactive groups in the exposed photoresist to react with a silicon-containing amine to achieve silicon incorporation into the resist polymer.

Selective diffusion of silicon into the imaged resist gained widespread attention with the DESIRE process introduced by Roland and co-workers [82,83]. Many derivative processes were later developed and given suitable acronyms, such as PRIME [84], SUPER [85], and SAHR [86]. All are single-layer patterning techniques that depend on preferential incorporation of a silicon-containing compound into the photoresist after the exposure step, Silicon incorporation in the resist was initially achieved by diffusion from the gas phase; however, Shaw et al. [87] introduced the use of a wet silylation process to produce an etch-resistant top resist layer. LaTulipe et al. [88,89] also used a liquid silylation process for surface imaging of a novolac resist. Silicon functionalization of a single-layer resist after exposure offers the attractive potential of simplifying both the resist processing sequence and the resist formulations. Although the various techniques differ in the exact mechanism of creating the contrast between the areas of silicon incorporation and silicon exclusion, many of the general characteristics are similar. Therefore, a detailed consideration of one of these schemes will serve to illustrate the major process parameters and concerns for this type of process.

12.8.1 The Desire Process

DESIRE, which is an acronym for diffusion-enhanced silylated resist, was the first commercialized surface imaging process [90–92]. Formulated originally for g-line exposure (436 nm), the technique is readily adaptable for I-line (365 nm) [93] as well as DUV (248 nm) [94,95] exposure. The DESIRE process, illustrated schematically in Figure 12.23, consists of four interdependent steps: (1) exposure and formation of the latent image, (2) presilylation bake, (3) formation of silylated image, and (4) dry etch transfer of the pattern. Successful patterning of the resist will depend on having optimized parameters for all four steps.

12.8.1.1 The Exposure Step

During the exposure step, the photoactive compound, a naphthoquinone diazide, undergoes photochemical decomposition. Since the unexposed photoactive compound is a diffusion inhibitor, the exposed resist is more susceptible to silicon diffusion. The exposure dose and shape of the projected image to a large degree determine the ultimate depth and lateral dispersion of the silicon incorporation into the resist.

12.8.1.2 The Presilylation Bake

The presilylation bake (step 2, Figure 12.23) is extremely important for selective incorporation of the silicon into the exposed regions. During this high-temperature bake, phenol ester formation by the unexposed photoactive compound forms a cross-linked and hence less permeable resist [91]. This thermally induced cross-linking of the unexposed resist in conjunction with the photochemical decomposition of the sensitizer in the exposed area leads to preferential silicon incorporation into the exposed areas. The temperature and duration of the presilylation bake and the silicon exposure steps are important for defining the contrast between the exposed and unexposed region [96].

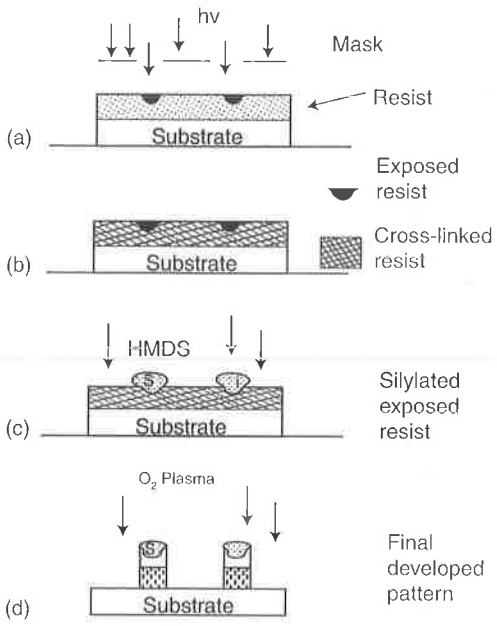

FIGURE 12.23
Schematic illustration of the DESIRE surface imaging process. (a) Exposure; (b) presilylation bake and cross linking; (c) silicon incorporation; and (d) oxygen plasma development.

12.8.1.3 Silicon Incorporation Step: Vapor Phase Silylation

Incorporation of silicon is typically performed by vapor-phase introduction of a suitable silicon-containing reagent such as hexamethyldisilazane (HMDS). The mechanism for diffusion of the gas-phase silylation agent has been widely investigated. The unexposed naphthoquinone diazide can act as a diffusion inhibitor for HMDS in a phenolic resin, while the exposed naphthoquinone diazide will increase the diffusion rate [97,98]. Generally, the resin must provide sufficient binding sites and the diffusion of the silicon must allow 8%–10% silicon incorporation, by weight, to provide sufficient etch selectivity [91]. Thermal crosslinking of the resist, initiated by the presilylation bake, continues during the silylation bake, and determines the permeability of the silicon delivery agent and, hence, selectivity. The presilylation and silylation bake parameters of temperature and time are sensitive controls for silicon incorporation. In addition, the chemical structure of the silylation agent will influence the diffusion rate and the total amount of silicon introduced into the resist. Early versions of the resist for the DESIRE process exhibited pattern deformation due to the volume change upon inclusion of the silylating agent in the resist. Changes in the resist polymer and optimization of the silylating agent have eliminated this problem [99,100].

Although HMDS is the most readily available silylating agent in semiconductor purity and was used most often for silylation processes, interesting alternative silylation agents have been investigated [93]. Small silylating agents such as dimethylsilyl dimethylamine (DMSDMA) and tetramethyldisilazane (TMDS) require relatively low temperatures (80°C–120°C), but silylating agents containing bulky groups such as 1,3-diisobutyl-1,1,2,2,-TMDS proved too bulky to provide sufficient silylation. For the smaller silicon delivery agents, it is important to decouple the presilylation bake from the silylation to obtain sufficient crosslinking and selectivity. Polyfunctional silylating agents have proven very attractive in certain applications [74,101].

12.8.1.4 Liquid-Phase Silylation

Although the silylating agent is usually introduced in the gas phase, liquid-phase silylation processes for DESIRE have been reported [102]. Liquid-phase silylation is carried out using a three-component system containing an inert carrier solvent (xylene), a diffusion promoter (*N*-methylpyrrolidone or propyl-eneglycol monomethyl ether acetate), and a silylating agent. Hexamethylcyclotrisilazane (HMCTS), a trifunctional cyclic amine, is generally used as the silylation agent [87,89,103], although monofunctional silylating agents such as bis(dimethylamino)dimethylsilane have also been used [102]. Hexamethylcyclotrisilazane induces crosslinking of the resin, which can reduce the silicon diffusion rate and ultimately limit the total silicon uptake. However, the crosslinking is beneficial because it prevents lateral swelling and pattern deformation as well as out-diffusion of silicon, problems that occur under certain conditions with gas-phase silylation [99,100,104].

Unlike gas-phase silylation, the liquid-phase silicon uptake exhibits a nonlinear response to exposure dose. There is a threshold behavior with exposure dose that should favor a more selective silylation process. The amount of silicon incorporated into the film for liquid-phase silylation (~25%) is much higher than in the gas-phase process (~10%). Hence, the dry-etch selectivity of these films is also higher [105]. The reason for the higher silicon content in the liquid silylation systems is not certain. Because the amount of observed silicon added to the resist corresponds to an average of two silicon atoms for each OH group, it is proposed that some polymerization, perhaps growth of polysiloxane chains on the phenolic OH group, occurs [105].

Liquid silylation techniques have applied to other surface imaging techniques [88,89] and hold promise for improved silylation processes. For implementation in device manufacturing, an aqueous-based solution such as that used for the CARL process is much preferred to a xylene-based system from the standpoint of compatibility with existing resist processes and environmental concerns.

12.8.1.5 Dry Etch Development

Dry-etch pattern transfer in the DESIRE process involves the use of an O_2 plasma to remove the unprotected resist while forming an etch-resistant silicon oxide covering in the silicon-containing areas. The dry development etch is generally carried out in a high-density plasma containing either pure oxygen or oxygen and a fluorocarbon gas [106]. Anisotropy of the etch is ensured by using very low pressures and by applying a DC bias to the wafer. Etch conditions must maintain a balance between the chemical composition of the etch and physical sputtering. If care is taken to minimize the isotropic components of the etch, the resultant resist profile will depend to a large extent on the silylated profile (Figure 12.23).

Successful pattern definition during dry development involves a combination of etching of any unprotected resist and sputtering away of the silylating region [107–109]. For understanding the etch process, models that assume some competition between SiO_2 formation and sputtering of the film by ion bombardment can be applied [110,111]. Evidence for formation of silicon oxide hard mask in the silylated regions comes from x-ray photoelectron spectroscopy (XPS) investigations of silylated resist samples before and after plasma exposure, which reveal that the silicon content of the surface does not change appreciably while there is a dramatic increase in the oxygen level. Both carbon and silicon XPS peaks are shifted to higher energy, indicating extensive oxidation [86]. For the unprotected resist, the etching mechanism involves both chemical and ion induced etching. Clearly, oxygen atomic concentration, ion flux, and energy are important parameters for the etch. In addition, the glass transition temperature for the silylated resist

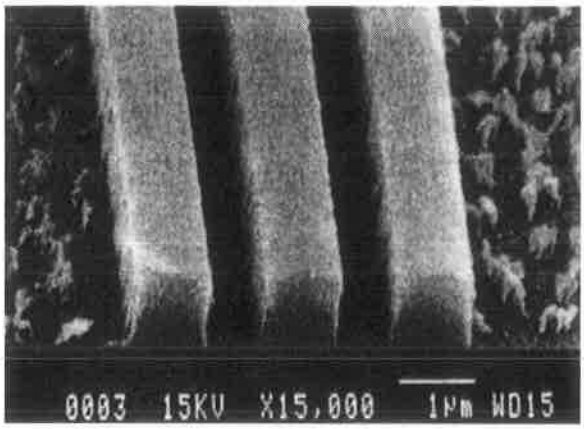

FIGURE 12.24
Examples of residue caused by unintentional silicon incorporation in exposed resist areas.

polymer (T_g) has been shown to be important [112]. At higher temperatures, silicon diffuses out of the exposed, silylated region, thus preventing adequate hard-mask formation. This is confirmed by silicon profiling studies and correlates with a dramatic decrease in the observed etch selectivity (initially silylated vs. unsilylated areas) with increasing wafer temperature during plasma development. Improvements in etch anisotropy with the use of very low temperatures (70°C) [113,114] and SO_2 in the plasma have been reported [115,116].

Initial attempts at dry development of silylated resists were plagued by severe problems with residue between patterned features and with line-edge roughness. Residue, sometimes referred to as *grass*, can arise from two sources: unintentional masking of resist during the plasma etch due to unwanted silicon incorporation in these areas, and sputtering and redeposition of materials. Residue caused by unintentional silylation is usually distributed equally throughout the pattern, in some instances appearing in greater abundance in large open areas. In contrast to this, residue from sputtering and redeposition is located almost exclusively between features that should be very well resolved by the exposure tool. An example of severe grass formation caused by parasitic silylation is illustrated in Figure 12.24.

Residue resulting from unintentional silicon incorporation can be minimized by optimizing the silylation and bake conditions to improve the selectivity of the silylation step. This usually involves changes in the bake time, temperature, pressure, or silylating agent. Alternatively, the dry development step can resolve the unwanted silicon inclusion by extending the overetch time (i.e., overdevelopment) or by introducing an initial nonselective etch step to remove a certain amount of resist uniformly from the wafer. The latter step, often referred to as a *descum*, involves the use of a fluorine-containing plasma or a high-energy ion-bombardment step [117,118]. Usually, an initial step with low selectivity for silylated resists is followed by a second, more selective etch [106]. A two-step oxygen etch, in which the initial step has a high ion energy, can also be used [117]. The disadvantage of either alteration of the dry development step is loss of resist thickness in the final pattern. This requires a thicker hard mask which usually translates into higher required exposure doses and longer processing times. Residue resulting from sputtering of the hard mask is eliminated by reducing the ion-bombardment energy in the plasma-development step.

Edge roughness for the dry-developed resist can be a serious concern, particularly as the dimensions of the line edge roughness become a significant percentage of the linewidth dimension. Extreme edge roughness is observed if the silicon content is insufficient to withstand the plasma dry development, and breakdown of the etch mask occurs.

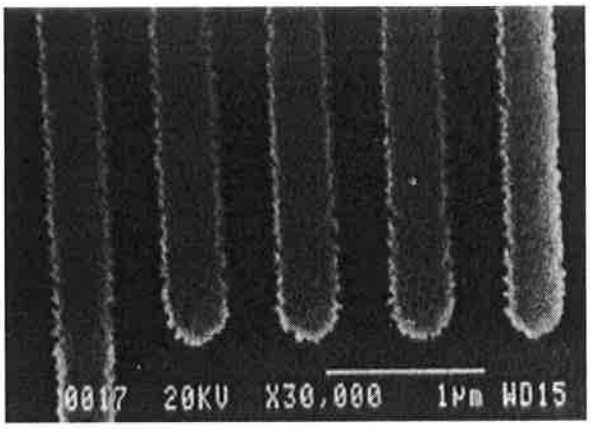

FIGURE 12.25
Line edge roughness resulting from hard mask breakdown during dry development of the resist.

The resist line roughness will most likely transfer into the underlying substrate during the subsequent etch step, causing variations in the pattern sizing. Severe edge roughness as illustrated in Figure 12.25 can be caused by insufficient silicon hard-mask protection of the underlying resist, low selectivity in the dry development etch, or both. Therefore, the silylation conditions and the dry-etch parameters must be optimized in concert to minimize the line roughness.

Hard-mask breakdown can also be observed when there is a lack of contrast in the exposed image. This can happen near the resolution limit of the exposure tool, or if the exposed image is severely defocused. Edge roughness is of special concern at 193 nm and shorter exposure wavelengths due to very shallow absorption depth of the resist coupled with the small targeted linewidths. Staining techniques that decorate the silylated resist profiles have verified the shallow silylated layer for these exposure wavelengths [75]. Any thinning of the silylated image near the edges of the silylated profile will result in an increase in line edge roughness. Figure 12.26 is a section of a silylated grating pattern that has been subjected to and oxygen plasma for a time sufficient to decorate the silylated areas but not completely etch the resist features. The oxygen etch has delineated the depth and lateral profile for the silylated regions [119]. It is interesting to note that edges of the silylated regions, some roughness is visible. The line edge roughness can be minimized by increasing the depth of silicon incorporation at the feature edges or by removing the thinner outer portions of the silicon hard mask during the dry development etch. The

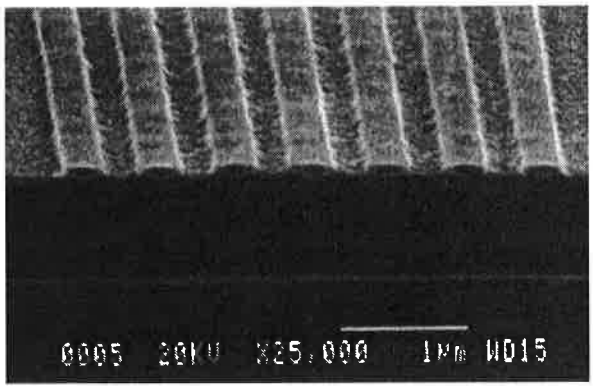

FIGURE 12.26
Silylated profiles (raised resist) which have been delineated using a short plasma etch.

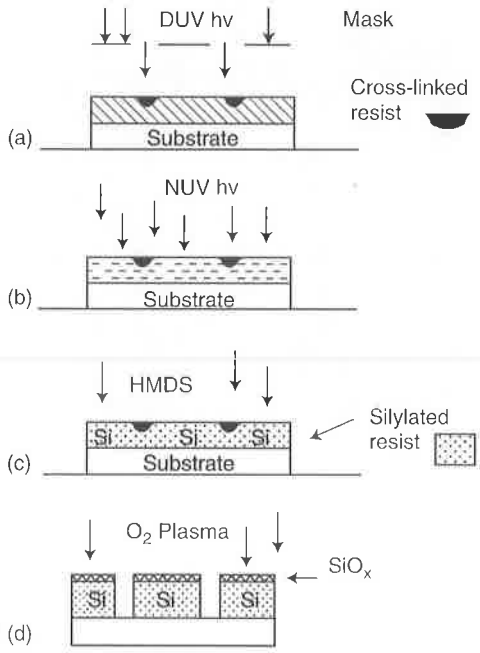

FIGURE 12.27
Schematic representation of the positive resist image by dry etching (PRIME) process. (a) Deep ultraviolet (DUV) exposure; (b) near UV (NUV) flood exposure; (c) presilylation bake and crosslinking; (d) silicon incorporation; and (e) oxygen plasma development.

latter solution leads to changes in CD with overetch and is not a good solution from the point of view of process control. Although there is speculation that the molecular-weight distribution of the resist could also influence the edge roughness, there have been no studies published to support this assertion.

12.8.2 The Positive Resist Image by Dry Etching (PRIME) Process

A variation of the DESIRE process for positive-tone images, called positive resist image by dry etching (PRIME), was developed by workers at LET [84,120,121]. The PRIME process uses the same resist as the DESIRE process and differs only in the addition of a second near-UV flood exposure step (Figure 12.27). Like a classical image reversal scheme, the PRIME process involve an initial exposure with DUV or e-beam followed by flood exposure at near UV wavelengths to produce a positive-tone image. During the initial exposure reaction of the photoactive compound results in crosslinking of the resist. For DUV exposure, only the top 300 Å of the resist is crosslinked, whereas the entire resist thickness is crosslinked upon e-beam exposure. Degradation of the photoactive compound during the subsequent near-UV flood exposure increases the diffusion rate of the silylation agent in the previously unexposed areas. Silylation and dry development are performed in a manner similar to that in the DESIRE process, the end result being a positive-tone image. A major difficulty with the PRIME process is the high energies required for both the crosslinking step (400 mJ/cm^2 at 248 nm and 300 mC/cm^2 for e-beam at 50 keV) and the flood exposure (1–2 J/cm^2). Although some work with more sensitive resist formulations has been reported [122], this still remains a serious concern.

12.8.3 The Silylated Acid Hardened Resist (SAHR) Process

The silylated acid hardened resist (SAHR) process (Figure 12.28) is a positive-tone single-layer process that relies on photoinitiated, acid-catalyzed crosslinking. In the SAHR

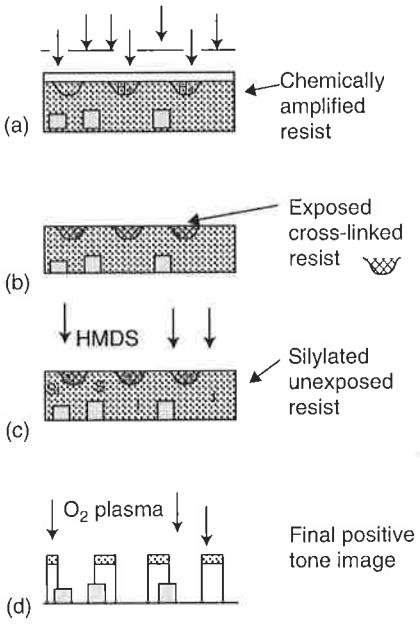

FIGURE 12.28
Silylated acid hardened resist process (SAHR). (a) Exposure and generation of photoacid; (b) postex posure bake and crosslinking of exposed resist; (c) silicon incorporation into unexposed resist; and (d) dry etch transfer of image.

process, DUV-induced acid generation in the imaging layer causes crosslinking in the exposed region during the postexposure bake step and renders these areas impermeable and unreactive to silylamines [123]. With gas-phase silylation, the unexposed resist incorporates 10%–12% silicon by weight, which is adequate to protect the underlying resist during the final plasma development.

The chemically amplified resists used in the SAHR process require much lover exposure doses (5–30 mJ/cm^2 for DUV exposures) compared with the novolac resists for the DESIRE process. The original SAHR process suffers from severe limitations with respect to its practical implementation. The first is the variation of silicon penetration depth with feature size, in which the larger features exhibit a much deeper silylation depth. This size-dependent variation of the silylated profiles make it difficult to control linewidth and maintain pattern-sizing linearity. The differential silicon incorporation cannot be explained simply by decreased optical contrast, as this effect is observed at feature sizes much larger than the resolution limit of the exposure tool. A plausible explanation is that the interfacial tension per unit volume becomes much larger as the patterned dimensions shrink, causing this sizing dependence [124]. An additional problem with the SAHR process is the resist flow during silylation. Incorporation of silyl groups into the resist film causes resist swelling and interferes with the hydrogen bonding, thus lowering the T_g of the resist film. As a consequence, during the silylation process the silylated resist overflows into the exposed (crosslinked) regions. This parasitic silicon incorporation degrades the silylation process contrast and requires extra processing steps to minimize the effect. Exposure of the resist to a bifunctional silane such as bis(dimethylamino)dimethylsilane prior to treatment with the silylating agent significantly diminishes the amount of silicon in the exposed areas by creating a thin crosslinked skin on the resist surface [124]. Alternatively, an aqueous development step prior to the silylation step eliminates both the flow problem and the size dependence of the silicon penetration depth. Surface depression in the unexposed areas are created by this development step and are refilled by the swollen silylated material.

However, this predevelopment step removes ~4000 Å of resist and requires thicker initial resist coatings.

Today, modified SAHR processes are being used with e-beam as well as shorter-wavelength (193- and 13.5-nm) exposure tools [101,114,125–127]. For these shorter-wavelength exposures, the crosslinking is facile due to the high photon energy. A number of patterning techniques have exploited this fact to create differential diffusion rates of a silicon-containing reagent to achieve surface imaging at 193 nm [125,128] or 13–40 nm (extreme UV [129]. For many of the 193-nm surface imaging techniques being explored, photochemical crosslinking, unaided by chemical amplification, is used [128].

12.8.4 Other Surface Imaging Techniques

Investigations targeted at developing surface imaging processes for high-resolution applications are yielding some interesting results. For example, work using plasma deposition of organosilicon shows promise for a single-layer and bilayer process [130–132]. An all-dry-patterning process involving the polymerization of methylsilane has demonstrated encouraging results with this thin conformal imaging layer [132]. In addition, nonsilicon-containing single-layer and bilayer processes are being investigated. Near-surface imaging using metal plating to define an etch-resistant mask has also been demonstrated [133–135]. In this process, a substrate surface is treated with an organosilane and exposed to DUV (248-nm) radiation. This exposure modifies the wettability of the substrate surface and reactivity of the surface and reactivity of the surface film. Subsequent treatment with a Pb/Sn catalyst followed by electroless copper and nickel metallization yields films several hundred angstroms thick in unexposed regions. This positive image can then be used as a plasma etch mask. The ultrathin films resulting from this process can lead to significant improvement in focal depth and resolution.

12.9 Use of Alternative Pattern Technology in Manufacturing

Surface imaging has traditionally been used to extend the capabilities of the current generation of optical lithography tools while allowing time for the newer tools to mature. Surface imaging or near-surface imaging techniques using bilayer approaches have found limited usage outside the research environment. There are, however, a few exceptions [73,136,137]. The DESIRE process was transferred to a pilot line at Texas Instruments and used in the early production and qualification of a 16-MB DRAM device [136]. The challenging topography and high reflectivity of the metal level necessitated the use of SIRs. The DESIRE process was eventually replaced by a process using conventionally developed resist; however, use of an antireflective coating (ARC) and enhanced planarization techniques were necessary to achieve performance comparable to that of the DESIRE process. It is of interest to note that the measured defect levels and yield for the DESIRE were comparable to those of the optimized ARC/conventional resist process [138]. As mentioned earlier, the CARL process has been used successfully at Seimens for manufacturing for a few years [73].

Antireflective coatings, both top and bottom layer films, are necessary for many current IC applications and are employed in numerous manufacturing lines. The manufacturing issues for nonconventional resist techniques such as surface imaging or bilayer resist imaging have been discussed by several authors [78,138,139]. However, the ultimate

selection of a photoresist process, whether conventional single-layer resist processing or one of the alternative processes discussed here, will depend on the achievable patterning resolution and process latitude robustness toward subsequent etching steps, linewidth control, ease of integration into current fabrication environments, yield, and ultimately cost.

12.9.1 Advantages and Disadvantages of Multilayer and Surface Imaging Techniques

Multilayer resist techniques and surface imaging processes are more complicated than conventional, single-layer, aqueous-developed resist techniques, but they have unique advantages. The improved depth of focus and resolution, insensitivity to topography, and ability to work with multiple stepper generations and wavelengths may, in certain applications, make them worth the added complications. The all-dry process allows very high aspect ratio resist patterning. Among the alternative methods for providing enhanced patterning capabilities, such as bilayer and trilayer processes [54,55,67], the single-layer SIR techniques are somewhat simpler from a processing standpoint.

The advantages outlined above must be weighed against the additional complexity of these alternative process. Nontraditional equipment is required for many of these techniques. For silylation-based processes, a silylation tool and a plasma etcher are required. Although the use of organic antireflective coatings has introduced etch processes into many formerly conventional patterning techniques, the silylation step has no equivalent in the conventionally developed resist process. The higher exposure dose requirement for some alternative techniques translates into lower throughput and higher costs. As with any plasma process, there are concerns about damage and defects caused by the dry-development plasma processing [140]. As device dimensions become smaller, additional concerns about the dry-development etch arise. For instance, edge roughness dimensions become a larger fraction of the linewidth and must be minimized. Damage mechanisms that may not have been detected with larger design sizes may become more important with the smaller device designs. Working close to or below the intended resolution of the stepper, as is often the case for many of the multilayer and surface imaging techniques, often increases the proximity effects. To minimize the proximity effects, the dry development must be carefully optimized. Still of major concern is that no manufacturing equipment set is available for many of these alternative processes.

12.9.2 Prognosis for Multilayer and Surface Imaging Technologies

Multilayer and surface imaging techniques will probably play an important role in future lithography development. These processes are easily applied to numerous exposure tools including 193-nm, e-beam, and EUV exposure systems. This is especially important for the development of new exposure tools where the resists are problematic [128,141]. Fortunately, many aspects of the process are the same across different wavelengths, so the experience gained with a tool set of one generation is readily adapted to the next-generation exposure tool. More variations are being added to the repertoire of available surface imaging or thin-film patterning processes. Both positive- and negative-tone silylated SIRs are now available [89,90,101]. Novel silylating agents are also being explored [101,102]. Improvements in the multilayer resist processes, particularly for application to 193-nm and EUV exposure, are ongoing. Optical enhancement techniques such as

modified illumination and phase shifting of reticles are complementary to near-surface and surface-imaging resist techniques and can further extend the process capabilities. Surface-imaging resist processing has become more widely known in the semiconductor industry. The equipment necessary for processing is becoming commercially available [42], and some of the nontraditional steps are becoming more familiar to lithographer because organic antireflective layers also require dry etching. In addition, the cost of implementing surface-imaging or multilayer resist processes can compare favorably with that of conventional processing if the cost of additional processes to compensate for the deficiencies of single-layer resist (e.g., antireflective coatings, etch hard masks) is considered.

References

1. L.E. Stillwagon and G.N. Taylor. 1989. "Polymers," in *Microlithogrpahy: Materials and Processes, ACS Symposium Series 412*, Washington, DC: American Chemical Society, pp. 252 265.
2. L.E. Stillwagon and R.G. Larsen. 1988. *Journal of Applied Physics Letters*, **63:** 5251.
3. J.J. Steigewald, S.P. Murarka, and R.J. Gutmann. 1997. Chemical Mechanical Planarization of Microelectronic Materials, New York: Wiley.
4. J.A. Bruce, B.J. Lin, D.L. Sundling, and T.N. Lee. 1987. *IEEE Transactions on Electron Devices*, **34:** 2428.
5. B.J. Lin, E. Bassous, W. Chao, and K.E. Petrillo. 1981. *Journal of Vacuum Science and Technology B*, **19:** 1313.
6. B.J. Lin. 1980. *Journal of the Electrochemical Society*, **127:** 202.
7. E.D. Lin, M.M. O'Toole, and M.S. Change. 1981. *IEEE Transactions on Electron Devices*, **28:** 1405.
8. C.H. Ting and K.L. Liauw. 1983. *Journal of Vacuum Science and Technology B*, **1:** 1225.
9. M.P. de Grandpre, D.A. Vidusek, and M.W. Leganza. 1985. *Proceedings of SPIE*, **539:** 103.
10. Y. Todokoro. 1980. *IEEE Transactions on Electron Devices*, **27:** 1443.
11. P.A. Lamarre. 1992. *IEEE Transactions on Electron Devices*, **39:** 1844.
12. E.D. Liu. 1982. *Solid State Technology*, **26:** 66.
13. C.H. Ting. 1983. *Proceedings of Kodak Interface 83*, **40**.
14. J.R. Havas. 1976. *The Electrochemical Society Extended Abstracts*, **2:** 743.
15. T. Brewer, R. Carlson, and J. Arnold. 1981. *Journal Applied Photographic Engineering*, **7:** 184.
16. R.D. Coyne and T. Brewer. 1983. *Proceedings of Kodak Interface 83*, **83:** 40.
17. Y. Mimura and S. Aoyama. 1993. *Microelectronic Engineering*, **21:** 47.
18. W. Ishii, K. Hashimoto, N. Itoh, H. Yamazaki, A. Yokuta, and H. Nakene. 1986. *Proceedings of SPIE*, 295 301.
19. C. Nölscher, L. Mader, and M. Scheegans. 1989. *Proceedings of SPIE*, **1086:** 242.
20. Such as Brewer Science ARC-XLN, Brewer Science Inc.
21. A. Reiser. 1989. *Photoreactive Polymers*, New York: Wiley, p. 323.
22. T.S. Yang, T. Koot, J. Taylor, W. Josphson, M. Spak, and R. Dammel. 1996. *Proceedings of SPIE*, **2724:** 724.
23. E. Pavelchek, J. Meudor, and D. Guerrero. 1996. *Proceedings of SPIE*, **2724:** 692.
24. H. Van Den Berg and J. Van Staden. 1979. *Journal Applied Physics*, **50:** 1212.
25. B. Martin and D. Gourley. 1993. *Microelectronic Engineering*, **21:** 61.
26. T. Ogawa, H. Nakano, T. Gocho, and T. Tsumori. 1994. *Proceedings of SPIE*, **2197**, 722 732.
27. Y. Tani, H. Mato, Y. Okuda, Y. Todokoro, T. Tatsuta, M. Sanai, and O. Tsuji. 1993. *Japanese Journal of Applied Physics*, **322:** 5909.
28. B.L. Draper, A.R. Mahoney, and G.A. Bailey. 1987. *Journal of Applied Physics*, **62:** 4450.
29. H. Tompkins, J. Sellars, and C. Tracy. 1993. *Journal Applied Physics*, **7:** 3932.
30. B. Smith, Z. Alam, and S. Butt. 1997. *Abstracts of the Second International Symposium on 193 nm Lithography*, Colorado Springs.
31. K.R. Dean, R.A. Carpio, and G.F. Rich. 1995. *Proceedings of SPIE*, **2438:** 514.

32. B.W. Smith, S. Butt, Z. Alam, S. Kurinec, and R. Lane. 1996. *Journal Vacuum Science and Technology B*, **14:** 3719.
33. R.E. Hummel. 1993. *Electronic Properties of Materials*, New York: Springer, pp. 186 230.
34. E.C. Palik. 1985. *Handbook of optical constants of solids I*, New York: Academic Press.
35. B.W. Smith, S. Butt, and Z. Alam. 1996. *Journal of Vacuum Science and Technology B*, **14:**6, 3714.
36. R.A. Cirelli, G.R. Weber, A. Komblit, R.M. Baker, F.P. Klemens, and J. DeMacro. 1996. *Journal of Vacuum Science and Technology B*, **14:** 4229.
37. C. Bencher, C. Ngai, B. Roma, S. Lian, and T. Vuong. 1997. *Solid State Technology*, **20:** 109.
38. T.A. Brunner. 1991. *Proceedings of SPIE*, **1466:** 297.
39. T. Tanaka, N. Hasegawa, H. Shiraishi, and S. Okazaki. 1990. *Journal of the Electrochemical Society*, **137:** 3900.
40. N. Bobroff and A. Rosenbluth. 1988. *Journal of Vacuum Science and Technology B*, **6**, 403 408.
41. T.A. Brunner. 1991. *Proceedings of SPIE*, **1466:** 297.
42. H. Shiraishi and S. Okazaki. 1991. *Proceedings of SPE Regional Technical Conference on Photopolymers*, Ellenville, NY, p. 195.
43. C.F. Lyons, R.K. Leidy, and G.B. Smith. 1992. *Proceedings of SPIE*, **1674:** 523.
44. D. Bernard and H. Arbach. 1991. *Journal of the Optical Society of America*, **8:** 123.
45. J.R. Havas. 1972. U.S. Patent 4,025,191.
46. A.F. Wiebe. 1970. U.S. Patent 3,511,652.
47. B.F. Griffing and P.R. West. 1983. *Polymer Engineering and Science*, **23:** 947.
48. D.C. Hofer, R.D. Miller, and C.G. Willson. 1984. *Proceedings of Microcircuit Engineering*, **A5** 1.
49. L.F. Halle. 1985. *Journal of Vacuum Science and Technology*, **3:** 323.
50. M. Endo, Y. Tani, M. Sasago, N. Nomura, N. Nomura, and S. Das. 1989. *Journal of Vacuum Science and Technology B*, **7:** 1072.
51. J.R. Havas. 1973. U.S. 3,873,361.
52. B.J. Lin and T.H.P. Change. 1979. *Journal of Vacuum Science and Technology*, **1:** 1969.
53. J.M. Moran and D. Maydan. 1979. *Journal of Vacuum Science and Technology*, **16:** 1620.
54. F. Buiguez, P. Parrens, and B. Picard. 1983. *Proceedings of SPIE*, **393:** 192.
55. B. Lin. 1983 in *Introduction to Microlithography*, L. Thompson, M. Bowden, and G. Wilson, eds., Washington, DC: American Chemical Society, pp. 287 349.
56. E. Bassous, L. Ephrath, G. Paper, and S. Mikalsen. 1983. *Journal of the Electrochemical Society*, **130:** 478.
57. M. Hatzakis, J. Paraszcak, and J. Shaw. 1981. *Proceedings of the Microelectronic Engineering Conference*, Lausanne, p. 386.
58. M. Hatzakis, J. Shaw, E. Babich, and J. Paraszczak. 1988. *Journal of Vacuum Science and Technology B*, **6:** 2224.
59. M. Hatzakis, J. Shaw, E. Babich, and J. Paraszczat, 1988. J. Vac. Sci. Technol. B, **6**, 2224.
60. G.N. Taylor, L.E. Stillwagon, and T. Venkatesan. 1984. *Journal of the Electrochemical Society*, **131:** 1658.
61. T.M. Wolf, G.N. Taylor, T. Venkastesan, and R.T. Kraetsch. 1984. *Journal of the Electrochemical Society*, **131:** 1664.
62. G.N. Taylor and T.M. Wolf. 1980. *Polymer Engineering and Science*, **20:** 1087.
63. C.W. Wilkins, E. Reichmanis, T.M. Wolf, and B.C. Smith. 1985. *Journal of Vacuum Science and Technology B*, **3:** 306.
64. Y. Saotome, H. Gokan, K. Sargo, M. Suzuki, and J. Ohnishi. 1985. *Journal of the Electrochemical Society*, **132:** 909.
65. R.D. Miller, D. Hofer, D.R. McKean, C.G. Willson, R. West, and P.T. Trefonas. 1984. in *Materials for Microlithography*, L.F. Thompson, C.G. Willson, and J.M.J. Frechet, eds., ACS Symposium Series 266, Washington, DC: American Chemical Society, pp. 293 310.
66. E. Reichmanis, S.A. MacDonald, and T. Iwayanagi. 1989. *Polymers in Microlithography*, Washington, DC: American Chemical Society.
67. R.D. Miller and G. Wallraff. 1994. *Advanced Materials for Optics and Electronics*, **4:** 95.
68. G.M. Wallraff, R.D. Miller, N. Clecak, and M. Baier. 1991. *Proceedings of SPIE*, **1466:** 211.
69. U. Schaedeli, E. Tinguely, A.J. Blakeney, P. Falcigno, and R.R. Kunz. 1996. *Proceedings of SPIE*, **2724:** 344.

70. R. Sezi, M. Sebald, R. Leuschner, H. Ahne, S. Birkle, and H. Borndorfer. 1990. *Proceedings of SPIE*, **1262:** 84.
71. M. Sebald, J. Berthold, M. Beyer, R. Leuschner, C. Noelscher, U. Scheler, R. Sezi, H. Ahne, and S. Birkle. 1991. *Proceedings of SPIE*, **1466:** 227.
72. M. Sebald, R. Leuschner, R. Sezi, H. Ahne, and S. Birkle. 1990. *Proceedings of SPIE*, **1262:** 528.
73. R.H. Leuschner, U. Marquardt, U. Nickel, E. Schmidt, E. Sebald, and R. Sezi. 1993. *Microelectronic Engineering*, **20:** 305.
74. W.C. McColgin, J. Jech, R.C. Daly, and T.B. Brust. 1987. *Proceedings of the Symposium on VLSI Technology* 9.
75. D.R. Wheller, S. Hutton, S. Stein, F. Baiocchi, M. Cheng, and G.N. Taylor. 1999. *Journal of Vacuum Science and Technology B*, **11:** 2789.
76. G. Taylor, R. Hutton, S. Stein, C. Boyce, O. Wood, B. Lafontaine, A. MacDowell et al. 1995. *Proceedings of SPIE*, **2437:** 308.
77. M.W. Horn, B.E. Maxwell, R.R. Knuz, M.S. Hibbs, L.M. Eriksen, S.C. Palmateer, and A.R. Forte. 1995. *Proceedings of SPIE*, **2438:** 760.
78. L.P. McDonnell Bushnell, L.V. Gregor, and C.F. Lyons. 1986. *Solid State Technology*, **June:** 133.
79. K.P. Miller and H.S. Sachdev. 1992. *Journal of Vacuum Science and Technology B*, **10:** 2560.
80. S.A. MacDolnald, H. Schlosser, H. Ito, J. Clecak, and C.G. Willson. 1991. *Chemistry of Materials*, **3:** 435.
81. H. Ito, S.A. MacDonald, R.D. Miller, and C.G. Willson. 1985. U.S. Patent 4,552,833.
82. F. Coopmans and B. Ronald. 1986. *Proceedings of SPIE*, **631:** 34.
83. B. Roland and A. Vrancken. 1985. European Patent Application 85,870,142.8.
84. C. Pierrat, S. Tedesco, F. Vinet, M. Lerme, and B. Dal'Zotto. 1989. *Journal of Vacuum Science and Technology B*, **7:** 1782.
85. C.M.J. Mutsaers, F.A. Vollenbroek, W.P.M. Nijssen, and R.J. Visser. 1990. *Microelectronic Engineering*, **11:** 497.
86. E.K. Pavelchek, J.F. Bohland, J.W. Thackery, G.W. Orsula, S.K. Jones, B.W. Dudley, S.M. Bobbio, and P.W. Freeman. 1990. *Journal of Vacuum Science and Technology B*, **8:** 1497 1501.
87. J.M. Shaw, M. Hatzakis, E.D. Babich, J.R. Paraszczak, D.F. Witman, and K.J. Stewart. 1989. *Journal of Vacuum Science and Technology B*, **7:** 1709.
88. D.C. La Tulipe, A.T.S. Pomerene, J.P. Simons, and D.E. Seeger. 1992. *Microelectronic Engineering*, **17:** 265.
89. D.C. LaTulipe, J.P. Simons, and D.E. Seeger. 1994. *Proceedings of SPIE*, **2195:** 372.
90. F. Coopmans and B. Roland. 1986. *Proceedings of SPIE*, **631:** 34.
91. B. Roland, R. Lombaerts, C. Jacus, and F. Coopmans. 1987. *Proceedings of SPIE*, **771:** 69.
92. R.J. Visser, J.D.W. Schellenkens, M.E. Reuhman-Huiskens, and L.J. Ijzendoorn. 1987. *Proceedings of SPIE*, **771:** 110.
93. K.H. Baik, L. Van Den Hove, A.M. Goethals, M. Op de Beeck, and R. Roland. 1990. *Journal of Vacuum Science and Technology B*, **8:** 1481.
94. M. Op de Beeck and L. Van Den Hove. 1992. *Journal of Vacuum Science and Technology B*, **10:** 701.
95. M.A. Hanratty and M.C. Timpton. 1992. *Proceedings of SPIE*, **1674:** 894.
96. A.M. Goethals, R. Lombaerts, B. Roland, and L. Van Den Hove. 1991. *Microelectronic Engineering*, **13:** 37.
97. B. Roland, R. Lombaerts, J. Vandendriessche, and F. Godts. 1990. *Proceedings of SPIE*, **1262:** 151.
98. B. Roland, J. Vandendriessche, R. Lombaerts, B. Denturck, and C. Jakus. 1988. *Proceedings of SPIE*, **920:** 120.
99. A.M. Goethals, D.N. Nichols, M. Op de Beeck, P. De Geyter, K.H. Baik, L. Van Den Hove, B. Roland, and R. Lombaerts. 1990. *Proceedings of SPIE*, **1262:** 206.
100. A.M. Goethals, K.H. Baik, K. Ronse, L. Van Den Hove, and B. Roland. 1993. *Microelectronic Engineering*, **21:** 239.
101. D. Wheeler, R. Hutton, C. Boyce, S. Stein, R. Cirelli, and G. Taylor. 1995. *Proceedings of SPIE*, **2438:** 762.
102. K.H. Baik, L. Van Den Hove, and B. Roland. 1991. *Journal of Vacuum Science and Technology B*, **9:** 3399.

103. M.E. Rouhman-Huisken, C.M.J. Mutsaers, F.A. Vollenbroek, and J.A. Moonen. 1989. *Microelectronic Engineering*, **9:** 551.
104. T.T. Doa, C.A. Spence, and D.W. Hess. 1991. *Proceedings of SPIE*, **1466:** 257.
105. K.H. Baik, K. Ronse, L. Van Den Hove, and B. Roland. 1992. *Proceedings of SPIE*, **1672:** 362.
106. R. Lombaerts, B. Roland, A.M. Goethals, and L. Van Den Hove. 1990. *Proceedings of SPIE*, **1262:** 43.
107. H.J. Dijkstra. 1992. *Journal of Vacuum Science and Technology B*, **10:** 2222.
108. P. LaPorte, L. Van Den Hove, and Y. Melaku. 1991. *Microelectronic Engineering*, **13:** 469.
109. C.M. Garza, G. Misium, R.R. Doering, B. Roland, and R. Lombaerts. 1989. *Proceedings of SPIE*, **1896:** 229.
110. F. Watanabe and Y. Ohnishi. 1986. *Journal of Vacuum Science and Technology B*, **4:** 422.
111. M.A. Hartney, D.W. Hess, and D.S. Soane. 1989. *Journal of Vacuum Science and Technology B*, **7:** 1.
112. P.J. Paniez, O.P. Joubert, M.J. Pons, J.C. Oberlin, T.G. Vachette, A.P. Weill, J.H. Pelletier, and C. Fiori. 1991. *Microelectronic Engineering*, **13:** 57.
113. C.W. Jurgensen, R.S. Hutton, and G.N. Taylor. 1992. *Journal of Vacuum Science and Technology B*, **10:** 2542.
114. S.C. Palmateer, R.R. Knuz, M.W. Horn, A.R. Forte, and M. Rothschild. 1995. *Proceedings of SPIE*, **2438:** 455.
115. M. Pons, J. Pelletier, and O. Joubert. 1994. *Journal of Applied Physics*, **75:** 4709.
116. R.S. Hutton, C.S. Boyce, and G.N. Taylor. 1995. *Journal of Vacuum Science and Technology B*, **13:** 236.
117. B. Roland, R. Lombaerts, and F. Coopmans. 1988. *Dry Process Symposium, 98*.
118. R.S. Hutton, R.L. Kostelak, O. Nalamasu, A. Kornbit, G. McNevin, and G. Taylor. 1990. *Journal of Vacuum Science and Technology B*, **8:** 1502.
119. G.R. Misium, M.A. Douglas, C.M. Garza, and C.B. Dobson. 1990. *Proceedings of SPIE*, **1262:** 74.
120. C. Pierrat, S. Tedesco, F. Vinet, M. Lerme, and B. Dal'Zotto. 1989. *Proceedings of Journal Vacuum Science*, **7:** 1782.
121. C. Pierrat, S. Tedesco, F. Vinet, T. Mourier, M. Lerme, B. Dal'Zotto, and J.C. Guiben. 1990. *Microelectronic Engineering*, **11:** 507.
122. F. Vinet, M. Chevallier, C. Pierrat, J.C. Guibert, C. Rosilio, and B. Mouanda. 1991. *Proceedings of SPIE*, **1466:** 558.
123. J.W. Thackeray, J.F. Bohland, E.K. Pavelchek, G.W. Orsula, A.W. McCullough, S.K. Jones, and S.M. Bobbio. 1990. *Proceedings of SPIE*, **1185:** 2.
124. G.S. Calabrese, J.F. Bohland, E.K. Pavelchek, R. Sinta, B.W. Dudley, S.K. Jones, and P.W. Freeman. 1993. *Microelectronic Engineering*, **21:** 231.
125. M. Hartney, R.R. Kunz, D. Ehrlich, and D. Shaver. 1990. *Proceedings of SPIE*, **1262:** 119.
126. M. Irmscher, B. Hoefflinger, R. Springer, C. Stauffer, and W. Peterson. 1996. *Proceedings of SPIE*, **2724:** 564.
127. T. Ohfuji and N. Aizaki. 1994. *Digest of Technical Papers-Symposium on VLSI Technology* 93.
128. M.A. Hartney, R.R. D, J. Ehrlich, and D.C. Shaver. 1990. *Journal of Vacuum Science and Technology B*, **8:** 1476.
129. H. Oizumi, Y. Yamashita, and M. Ohtani. 1996. *Microelectronic Engineering*, **30:** 291.
130. M.W. Horn, S.W. Pang, and M. Rothschild. 1991. *Journal of Vacuum Science Technology B*, **8:** 149.
131. T.W. Weidman and A.M. Joshi. 1993. *Applied Physics Letters*, **62:** 372.
132. R.L. Kostelak, T.W. Weidman, S. Vaidya, O. Joubert, S.C. Palmateer, and M. Habbs. 1995. *Journal of Vacuum Science and Technology B*, **13:** 2994.
133. M.L. Schilling, H.E. Katz, F.M. Houlihan, S.M. Stein, R.S. Hutton, and G.N. Taylor. 1996. *Journal of the Electrochemical Society*, **143:** 691.
134. G.S. Calabrese, L.N. Abali, J.F. Bohland, E.K. Pavelchek, P. Sricharocenchaikit, G. Vizvary, S.M. Bobbio, and P. Smith. 1991. *Proceedings of SPIE*, **1466:** 528.
135. J. Calvert, M. Chen, C. Dulcey, J. George, M. Peckerar, O. Schnur, and P. Schoen. 1991. *Journal of Vacuum Science and Technology B*, **9:** 3447.
136. C.M. Garza, D.L. Catlett, and R.A. Jackson. 1991. *Proceedings of SPIE*, **1466:** 616.
137. M.C. Tipton and M.A. Hanaratty. 1992. *Microelectronic Engineering*, **17:** 47.
138. C.M. Garza, E.J. Solowiej, and M.A. Boehm. 1992. *Proceedings of SPIE*, **1672:** 403.

139. D.E. Seeger, D.C. La Tulipe, R.R. Kunz, C.M. Garza, and M.A. Hanaratty. 1997. *IBM Journal of Research and Development*, **41:** 105.
140. S.J. Fonash, C.R. Viswanathan, and V.D. Chan. 1994. *Solid State Technology*, **37:**7, 5.
141. R.D. Allen, G.M. Wallraff, D.C. Hofer, R.R. Kunz, S.C. Palmateer, and M.W. Horn. 1995. *Microlithography World*, **Summer:** 21.
142. B.J. Park, K.H. Baik, H.K. Kim, J.W. Kim, C.K. Bok, J. Vertommen, and R. Rosenlund. In press. Proceedings of SPIE.